Check for updates

JGR Oceans

RESEARCH ARTICLE
10.1029/2026JC024641

Meltwater Pathways Control the Effect of Subglacial Discharge on Sub-Shelf Melting

Franka Jesse[1], Erwin Lambert[2], Paul R. Holland[3], Kaitlin A. Naughten[3], Constantijn J. Berends[1], and Roderik S. W. van de Wal[1,2,4]

[1]Utrecht University Science Faculty, Utrecht, The Netherlands, [2]Royal Netherlands Meteorological Institute (KNMI), De Bilt, The Netherlands, [3]British Antarctic Survey, Cambridge, UK, [4]Utrecht University Department of Physical Geography, Utrecht, The Netherlands

Key Points:

- Meltwater-layer model LADDIE reproduces enhanced sub-shelf melting driven by subglacial freshwater discharge, as simulated by MITgcm
- LADDIE is used to assess the effect of ocean conditions and freshwater release location on the melting enhancement by subglacial discharge
- Release location is key: divergent meltwater pathways amplify integrated melting through broader spreading of buoyant meltwater

Supporting Information:

Supporting Information may be found in the online version of this article.

Correspondence to:

F. Jesse,
t.f.jesse@uu.nl

Citation:

Jesse, F., Lambert, E., Holland, P. R., Naughten, K. A., Berends, C. J., & van de Wal, R. S. W. (2026). Meltwater pathways control the effect of subglacial discharge on sub-shelf melting. *Journal of Geophysical Research: Oceans*, *131*, e2026JC024641. https://doi.org/10.1029/2026JC024641

Received 25 MAY 2026
Accepted 12 NOV 2026

Author Contributions:

Conceptualization: Franka Jesse, Erwin Lambert, Paul R. Holland, Kaitlin A. Naughten, Roderik S. W. van de Wal
Data curation: Franka Jesse
Formal analysis: Franka Jesse, Paul R. Holland, Kaitlin A. Naughten
Investigation: Franka Jesse
Methodology: Franka Jesse, Erwin Lambert, Paul R. Holland, Kaitlin A. Naughten, Roderik S. W. van de Wal
Software: Franka Jesse, Erwin Lambert, Paul R. Holland, Constantijn J. Berends

© 2026 The Author(s). Journal of Geophysical Research: Oceans published by Wiley Periodicals LLC on behalf of American Geophysical Union.
This is an open access article under the terms of the Creative Commons Attribution License, which permits use, distribution and reproduction in any medium, provided the original work is properly cited.

Abstract Increased ocean-driven ice-shelf melting is a major contributor to mass loss from the Antarctic Ice Sheet. When subglacial freshwater discharge (SFD) enters ice-shelf cavities, it enhances local buoyancy and accelerates meltwater flow beneath ice shelves and increases melt rates. We adapt the meltwater-layer model LADDIE to include SFD and show that it quantitatively reproduces the melt sensitivity to SFD of the more complex three-dimensional ocean model MITgcm for the Thwaites ice shelf cavity. We then use the adapted LADDIE model to investigate the sensitivity of SFD-enhanced melting to (a) background ocean conditions and (b) SFD release location. We focus on the Thwaites and Pine Island ice shelves, which experience substantial ocean-driven melting and both receive SFD in their cavities, but have distinctly different geometries. Our results show that SFD-enhanced melting is relatively insensitive to ocean conditions representing present-day variability and projected 50-year warming. Instead, it is strongly controlled by the SFD release location. Ice-shelf geometry controls whether meltwater flow from the release site converges or diverges laterally across the ice base, shaping the magnitude and spatial pattern of additional melting. Divergent flow spreads buoyancy forcing over a larger area, producing stronger integrated melt enhancement than convergent flow, where forcing is concentrated. In the convergent-flow case, however, local increases in melting are higher, which may be important for the ice-dynamical response. These findings underscore the importance of accurately constraining the SFD release locations and resolving meltwater pathways when representing SFD-driven melting in ice-sheet projections.

Plain Language Summary Freshwater flowing beneath Antarctic glaciers is discharged into the ocean beneath ice shelves. This so-called subglacial freshwater discharge makes the ocean water more buoyant and strengthens the meltwater flow, increasing ice-shelf melting. However, it is still unclear how the ocean conditions and the location of freshwater discharge control the magnitude and pattern of this additional melting. To investigate this, we use a computer model designed to simulate meltwater flow beneath ice shelves. We focus on the Thwaites and Pine Island ice shelves in West Antarctica, which experience strong ocean-driven melting and receive freshwater discharge within their cavities. Our results show that the additional melting caused by freshwater discharge depends much more on where the freshwater enters the cavity than on the background ocean conditions. Different discharge locations create different patterns and amounts of additional melting because they strengthen different meltwater flow pathways beneath the ice shelf. Given that patterns of ice-shelf melting strongly influence estimates of future Antarctic ice mass loss, our results highlight the need to improve understanding of where subglacial freshwater enters ice-shelf cavities in order to more accurately represent its effect on melting in coupled ice-sheet–ocean models.

1. Introduction

The Antarctic Ice Sheet (AIS) has been losing mass at a rate of 106 ± 10 Gt yr^{-1} between 1979 and 2023, contributing a total of 13.3 ± 1.4 mm to global sea-level rise over this period (Otosaka et al., 2026). Much of this mass loss is concentrated in regions exposed to relatively warm, saline ocean waters that drive high sub-shelf melt rates and promote rapid ice-shelf thinning (Adusumilli et al., 2020; Rignot et al., 2019). This thinning reduces buttressing and enhances glacier discharge into the ocean (Dupont & Alley, 2005). Consequently, understanding ocean-driven sub-shelf melting is key to predicting future changes of the AIS (Beckmann et al., 2025).

The ocean circulation within ice-shelf cavities is primarily buoyancy driven (Lewis & Perkin, 1986). In many cases, warm, saline waters enter the cavity at depth and reach the grounding line, where they drive strong sub-

Supervision: Erwin Lambert, Roderik S. W. van de Wal
Validation: Franka Jesse
Visualization: Franka Jesse
Writing – original draft: Franka Jesse
Writing – review & editing: Franka Jesse, Erwin Lambert, Paul R. Holland, Kaitlin A. Naughten, Constantijn J. Berends, Roderik S. W. van de Wal

shelf melting. The resulting meltwater forms a buoyant, relatively fresh layer that flows along the ice-shelf base toward the open ocean. The pathway of this meltwater layer is strongly influenced by topographic steering, and melt rates depend on both thermal driving and friction velocity within the meltwater layer (Hewitt, 2020). Consequently, melt patterns are highly heterogeneous, with elevated melt rates typically occurring near grounding lines, where thermal forcing is strongest, and within basal channels, where friction velocities are amplified through topographic steering (Zinck et al., 2026).

The buoyancy-driven circulation beneath ice shelves can be modified by subglacial freshwater discharge (SFD), which enters ice-shelf cavities at discrete locations along the grounding line (Le Brocq et al., 2013). This freshwater originates from meltwater that accumulates beneath the grounded ice and is routed through channelized drainage networks that can discharge substantial freshwater fluxes into ice-shelf cavities (Hewitt, 2011). Several observational and modeling studies indicate that many major Antarctic glaciers are underlain by such drainage systems (Dow et al., 2020; Ehrenfeucht et al., 2025; Hager et al., 2022; Wearing et al., 2024; Wei et al., 2020). Due to its near-zero salinity, SFD is highly buoyant relative to the ambient ocean and can locally accelerate the meltwater flow along the ice-shelf base, strengthening the buoyancy-driven circulation and increasing friction velocities at the ice–ocean interface and thereby sub-shelf melt rates.

The influence of SFD on sub-shelf melting and cavity circulation has been investigated using cavity-resolving 3D ocean models. In simulations using idealized geometry and SFD forcing, Vaňková et al. (2025b) demonstrated that the total melt flux increases approximately with the two-thirds power of channelized SFD. Regional studies using realistic geometry and SFD forcing further highlight the importance of SFD across several Antarctic ice shelves. Gourmelen et al. (2025) simulated melt enhancement following a subglacial lake drainage event beneath Thwaites Glacier and identified a power-law relationship between melt amplification and channelized SFD with an exponent smaller than one (i.e., sub-linear), similar to that reported by Vaňková et al. (2025b). For Pine Island ice shelf, Nakayama et al. (2021) showed that including SFD substantially intensifies melting near the grounding line, bringing simulated melt rates closer to satellite-derived melt rates in that region, although the effect on total melt remains limited. Simulations of Totten ice shelf indicate that SFD enhances melting, both near the grounding line and further downstream, with the response primarily driven by enhanced circulation rather than additional ocean heat supply (Gwyther et al., 2023). In summary, these four ocean-modeling studies demonstrate that SFD can substantially alter both the magnitude and spatial distribution of sub-shelf melting.

While Vaňková et al. (2025b) explored the effects of varying ambient ocean conditions and different SFD release locations in idealized configurations, it remains unclear how SFD-enhanced melting responds to these factors in realistic ice-shelf geometries. Understanding the sensitivity to ambient ocean conditions could provide insight into the variability of SFD-enhanced melting and how its magnitude might change under future warming. Similarly, understanding the sensitivity to the SFD release location could indicate how precisely this location needs to be constrained when representing SFD in ice-sheet projections.

In this study, we employ the one-Layer Antarctic model for Dynamical Downscaling of Ice–ocean Exchanges (LADDIE), version 2.0 (Lambert et al., 2026), to investigate SFD-driven melt amplification by extending it to include SFD forcing. LADDIE 2.0 resolves the buoyancy-driven flow of the meltwater layer beneath ice shelves by averaging it over the vertical dimension, explicitly representing topographic steering and Coriolis deflection of the meltwater layer. By resolving only the boundary layer, LADDIE 2.0 substantially reduces computational cost compared to full 3D ocean models while retaining the key physical processes that control melt distribution. It produces melt patterns comparable to those simulated by cavity-resolving ocean models and provides an alternative to parameterizations currently used in ice-sheet models (Jesse et al., 2025). Here, we validate our model configuration against MITgcm simulations and then address the following research question for the Thwaites and Pine Island ice shelves: how sensitive is SFD-enhanced melting, in terms of spatial pattern and total melt flux, to (a) ambient ocean conditions and (b) the release location of SFD?

The remainder of this manuscript is structured as follows. Section 2 provides a detailed description of the study area, and Section 3 presents the LADDIE model and the experiment design. Section 4 covers the model evaluation. The results on the sensitivity of SFD-enhanced melting to ambient ocean conditions and to SFD release location are presented in Sections 5 and 6, respectively. Finally Sections 7 and 8 provide the discussion and conclusions.

21699291, 2026, 12, Downloaded from https://agupubs.onlinelibrary.wiley.com/doi/10.1029/2026JC024641 by British Antarctic Survey, Wiley Online Library on [27/11/2026]. See the Terms and Conditions (https://onlinelibrary.wiley.com/terms-and-conditions) on Wiley Online Library for rules of use; OA articles are governed by the applicable Creative Commons License

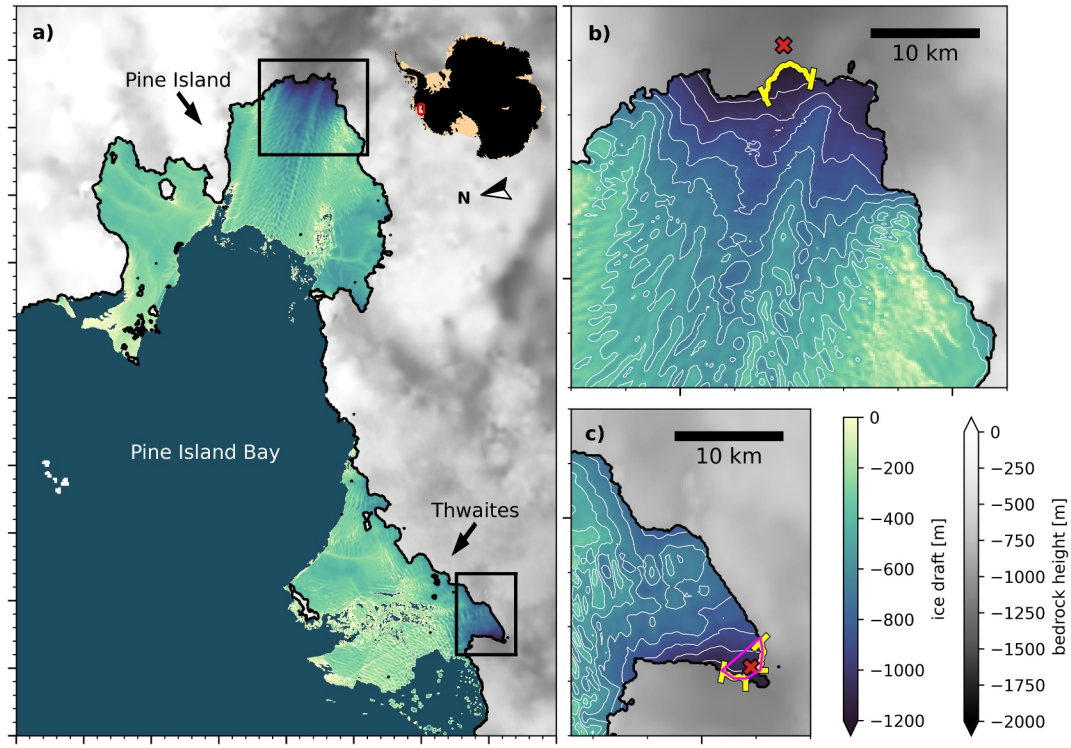


Figure 1. Map of the study area showing ice-shelf draft from TanDEM-X derived data (Bevan et al., 2021; P. Holland et al., 2023; Lowery et al., n.d.) and bedrock elevation from BedMachine v3 (Morlighem et al., 2020). The draft geometry corresponds to 2023 for Pine Island and 2013 for Thwaites (the latter as in Gourmelen et al. (2025)). Zoomed-in views of ice-shelf draft with added contours (spaced 100 m apart) are provided for the specific study regions of Pine Island (b) and Thwaites (c). The grounding line is shown in black. In panels (b, c), the red cross indicates the estimated location of subglacial discharge from Ehrenfeucht et al. (2025), and the yellow segments mark the reference SFD regions used in the LADDIE experiments. The magenta line in panel (c) encloses the location of release in MITgcm.

2. Study Area

We focus on two major outlet systems, Pine Island and Thwaites, in the Amundsen Sea sector of West Antarctica, a region that is currently one of the largest contributors to Antarctic mass loss (Shepherd et al., 2019). Mass loss in this sector is primarily driven by strong ocean-driven melting, as relatively warm Circumpolar Deep Water ($T \approx 1°C$) intrudes onto the continental shelf and enters Pine Island Bay (Kimura et al., 2017). From there, it accesses ice-shelf cavities including Pine Island and Thwaites (Figure 1a), contributing to high rates of sub-shelf melting (Dutrieux et al., 2014; P. Holland et al., 2023; Wåhlin et al., 2021). Regional climate projections indicate strong future warming of Pine Island Bay, with increasing ocean temperatures and a shoaling thermocline (Naughten et al., 2023).

Despite their shared oceanographic setting, the Pine Island and Thwaites ice shelves differ in their geometric configuration. The grounding zone of Pine Island is relatively broad and laterally extensive, and is incised by prominent basal channels aligned with the ice flow (Figure 1b). In contrast, the grounding zone of Thwaites is more laterally confined and lacks similarly well-developed channelized features (Figure 1c).

Increasing evidence suggests that SFD plays an important role in modulating sub-shelf melt rates beneath both ice shelves (Gourmelen et al., 2025; Nakayama et al., 2021). A pan-Antarctic modeling study indicates the presence of subglacial drainage outlets at their grounding lines (Ehrenfeucht et al. (2025); estimated locations indicated in Figures 1b and 1c). Regional estimates suggest steady-state SFD fluxes of approximately 50 $m^3\ s^{-1}$ for Pine Island (Zhang et al., 2024) and 80 $m^3\ s^{-1}$ for Thwaites (Malczyk et al., 2023). At Thwaites, SFD may additionally be influenced by upstream subglacial lake systems that can generate episodic drainage events. For example, a sequence of connected lakes drained in 2013, temporarily increasing discharge to approximately 640 $m^3\ s^{-1}$ (Gourmelen et al., 2025).

21699291, 2026, 12, Downloaded from https://agupubs.onlinelibrary.wiley.com/doi/10.1029/2026JC024641 by British Antarctic Survey, Wiley Online Library on [27/11/2026]. See the Terms and Conditions (https://onlinelibrary.wiley.com/terms-and-conditions) on Wiley Online Library for rules of use; OA articles are governed by the applicable Creative Commons License

21699291, 2026, 12, Downloaded from https://agupubs.onlinelibrary.wiley.com/doi/10.1029/2026JC024641 by British Antarctic Survey, Wiley Online Library on [27/11/2026]. See the Terms and Conditions (https://onlinelibrary.wiley.com/terms-and-conditions) on Wiley Online Library for rules of use; OA articles are governed by the applicable Creative Commons License

Taken together, the combination of similar ocean forcing, contrasting geometric configurations, and evidence for SFD makes the Pine Island and Thwaites systems well suited for investigating the role of SFD in influencing sub-shelf melting.

3. Methods

We use the meltwater-layer model LADDIE to simulate sub-shelf melt and its sensitivity to SFD beneath the Thwaites and Pine Island ice shelves. Existing simulations with the ocean model MITgcm serve two purposes. First, for Thwaites, they provide the reference against which LADDIE's response to SFD is evaluated (a perfect-model approach). The aim is to assess whether LADDIE captures the essential physics required to reproduce the SFD-induced melt response of the more complete model, rather than to claim that either model is more realistic. Second, for both ice shelves, the output from the MITgcm simulations is used to derive the ambient ocean conditions that force LADDIE. In Section 3.1, we therefore first describe the existing MITgcm simulations and the fields we extract from them. In Section 3.2, we then describe LADDIE and our SFD extension, followed by the evaluation of LADDIE against MITgcm for Thwaites and the sensitivity experiments for both ice shelves.

3.1. MITgcm Data for LADDIE Evaluation and Forcing

We analyze existing simulations performed with hydrostatic configurations of MITgcm for the Thwaites and Pine Island ice-shelf cavities, both at 200 m horizontal and 10 m vertical resolution. These configurations of MITgcm are forced at the open ocean boundaries using restoring profiles of temperature and salinity, and require bathymetry and ice-shelf geometry as external input data sets. Melt rates are computed with the three-equation parameterization (D. M. Holland & Jenkins, 1999; Jenkins et al., 2010), in which friction velocity and thermal driving are the key inputs. In MITgcm, these quantities are calculated using velocity, temperature, and salinity averaged over the upper 10 m beneath the ice. The boundary conditions and geometry for the two cavities are described below.

3.1.1. Thwaites MITgcm Simulations

For Thwaites, we consider a set of nine distinct steady-state MITgcm simulations of the Thwaites ice-shelf cavity presented in Gourmelen et al. (2025), which use a modified version of the model setup of P. Holland et al. (2023). In each simulation, SFD was prescribed as a freshwater volume flux ($S = 0.0$ psu, $T = -0.5$°C) distributed over the full water column within the deepest part of the Thwaites grounding line (magenta line, Figure 1c). The prescribed SFD flux ranged from 0 to 640 $m^3\ s^{-1}$ in increments of 80 $m^3\ s^{-1}$, spanning both the estimated steady-state discharge (~80 $m^3\ s^{-1}$) and the 2013 subglacial lake outburst (~640 $m^3\ s^{-1}$).

The ice-shelf cavity geometry represents conditions during the 2013 lake drainage event and is based on TanDEM-X data (Figure 1a). The ice-shelf draft was derived following Bevan et al. (2021) and P. Holland et al. (2023), combining TanDEM-X surface elevations with hydrostatic equilibrium assumptions after corrections for geoid offset, tides, and firn air content to determine floating ice thickness.

Restoring temperature and salinity profiles at the open boundaries were held constant, with a warm (+1.2°C) and saline (34.7 PSU) deep CDW layer below 600 m, overlain by a colder (−1°C) and fresher (34 PSU) Winter Water layer above 200 m. These restoring profiles were held constant across all simulations to ensure that differences in sub-shelf melt arise solely from variations in SFD forcing.

These simulations provide the primary benchmark for evaluating whether the melt response to SFD in LADDIE is consistent with that simulated by MITgcm. The simulation without SFD additionally provides the melt reference used to calibrate LADDIE, the three-dimensional temperature and salinity fields that force the LADDIE evaluation experiments, and the ambient profiles from which the idealized forcing for the Thwaites sensitivity experiments is derived.

3.1.2. Pine Island MITgcm Simulation

For Pine Island, we consider a single MITgcm simulation of the Pine Island ice-shelf cavity in which no SFD was prescribed. The model domain and settings are identical to those described by Lowery et al. (2026), but both the ocean boundary restoring and ice-shelf geometry differ from that study. The restoring profiles are identical to those used in the Thwaites simulations described above, while the ice-shelf cavity geometry is based on

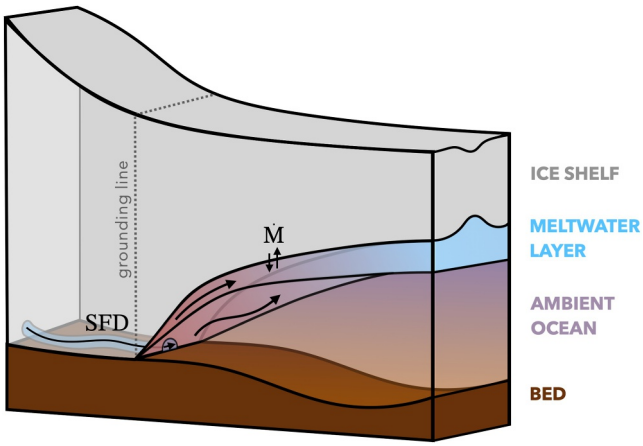


Figure 2. Schematic of the LADDIE model, illustrating the meltwater layer beneath the ice shelf. The model takes ice-sheet geometry and ambient ocean conditions as input. It has been extended to include subglacial freshwater discharge (SFD), which can be varied in both total flux and spatial distribution along the grounding line where it enters the cavity.

TanDEM-X data for 2023 (Figure 1a; Lowery et al., n.d.). Again, the ice-shelf draft was derived following Bevan et al. (2021) and P. Holland et al. (2023) from TanDEM-X surface elevations using hydrostatic equilibrium with standard geoid, tide, and firn corrections.

We use the ambient temperature and salinity fields from this simulation to construct idealized ocean forcing for the Pine Island sensitivity experiments with LADDIE.

3.2. Meltwater-Layer Model LADDIE

3.2.1. Model Description

We use the meltwater-layer model LADDIE version 2.0 (Lambert et al., 2026), which resolves the buoyancy-driven flow within the well-mixed meltwater layer based on two-dimensional, depth-averaged, plume dynamics (P. Holland & Feltham, 2006). It is designed to simulate steady-state sub-shelf melt patterns beneath ice shelves based on prescribed ice-shelf geometry and ambient ocean forcing. The latter can consist of 3D temperature and salinity fields from cavity-resolving models, or ice-front conditions (from non-cavity-resolving models or observations) extrapolated into the cavity following Jourdain et al. (2020). Density is computed from temperature and salinity using a linear equation of state.

Sub-shelf melt rates in LADDIE are computed using the same three-equation formulation as in MITgcm (D. M. Holland & Jenkins, 1999; Jenkins et al., 2010). The two models differ in the layer over which velocity, temperature, and salinity are averaged to obtain the friction velocity and thermal driving. Instead of the fixed 10 m layer beneath the ice used in MITgcm, LADDIE uses values averaged over the meltwater layer, whose thickness is solved for by the model and varies spatially (typically between about 1 and 10 m, but locally up to 100 m).

In the model, the meltwater layer is subject to several volume source terms: sub-shelf melting, entrainment of ambient ocean water, and an additional artificial entrainment term introduced to prevent the layer from becoming infinitely thin. Following Lambert et al. (2026), the minimum layer thickness is set to 1 m in this study. In regions of divergent flow, where melt and entrainment are insufficient to maintain this minimum thickness, this artificial entrainment term increases the entrainment of ambient ocean water to maintain layer stability. Both physical and artificial entrainment inherit the temperature and salinity of the ambient ocean, whereas meltwater is introduced at the local pressure-dependent freezing temperature with zero salinity.

A key extension introduced in this study is the representation of SFD (Figure 2). Following Gladish et al. (2012), who used a similar meltwater layer model, we represent SFD as an additional volume source term to the meltwater layer, rather than as a boundary condition imposing a velocity flux across the grounding line. In this sense, it is treated similarly to the volume source terms introduced above. In line with previous studies using regional 3D cavity-resolving ocean models (Goldberg et al., 2023; P. Holland et al., 2023; Vaňková et al., 2025b), the freshwater source is introduced at the local pressure-dependent freezing temperature and zero salinity. Unlike sub-shelf melting and entrainment, which are computed in all floating cells, SFD is applied only in cells along the grounding line that intersect a prescribed SFD mask. Using such a prescribed SFD mask allows the location and spatial extent of the discharge to be controlled, for example, by widening or narrowing the mask defining the release region. The total SFD flux is distributed among these cells in proportion to their area, ensuring a spatially uniform thickening of the meltwater layer resulting from the imposed freshwater input.

In contrast to MITgcm, where SFD is released over the full water column in the deeper part of the grounding zone, LADDIE adds the SFD directly to the meltwater layer at the first grounding-line cells. This reflects a modeling choice in LADDIE, representing discharge as a localized input where it enters the cavity, with its buoyancy acting directly on the meltwater layer. Alternatives, such as releasing the flux farther from the grounding line, or adding only part of it to the meltwater layer and using the remainder to modify the ambient conditions, are not implemented here but could be explored in future work.

21699291, 2026, 12, Downloaded from https://agupubs.onlinelibrary.wiley.com/doi/10.1029/2026JC024641 by British Antarctic Survey, Wiley Online Library on [27/11/2026]. See the Terms and Conditions (https://onlinelibrary.wiley.com/terms-and-conditions) on Wiley Online Library for rules of use; OA articles are governed by the applicable Creative Commons License

Table 1
Overview of the LADDIE Experiments

Experiment set	Ocean forcing	SFD location	SFD strength (m^3 s^{-1})	
			Thwaites	Pine Island
Model evaluation (Section 4)	smoothed, 3D spatially varying MITgcm fields	reference	0 to 640 in steps of 80	–
Ambient ocean sensitivity (Section 5)	reference + 4 perturbations (Figure 3)	reference	0, 80, 160, 320, 640	0, 50, 80, 160, 320, 640
SFD location sensitivity (Section 6)	reference	reference + 8 perturbations (Figure 4)	0, 80, 160, 320, 640	0, 50, 80, 160, 320, 640

Note. All experiments use the same drag coefficient tuning ($C_{d,\mathrm{top}} = 2.5 \times 10^{-3}$) and mesh resolution (maximum triangle edge length of 200 m). Ice shelf geometry is derived from TanDEM-X data, following the method by Bevan et al. (2021). For Thwaites, this geometry is representative of the year 2013, and for Pine Island of the year 2023. The reference ocean forcing is the horizontally uniform idealized T, S profile labeled reference in Figure 3, and the reference SFD location is the central 5 km release width labeled reference in Figure 4, both defined separately for each ice shelf.

The LADDIE domain spans the horizontal extent of the ice shelf and is implemented on an unstructured mesh (Berends et al., 2025). The configurations used in this study employ a maximum triangle edge length of 200 m, resulting in a mean cell area of just under 26,000 m^2 and an effective resolution of around 160 m, with a time step of 20 s. A run duration of 10 model days was used for all LADDIE simulations. Sensitivity tests showed this duration to be sufficient to reach steady state for both the Thwaites and Pine Island meltwater layers, owing to the short flushing timescales of the meltwater layer in relatively warm, small ice-shelf cavities. This meltwater flushing time is shorter than that of the full ice-shelf cavity, as the meltwater layer occupies a much smaller volume and exhibits higher flow speeds (P. Holland, 2017). Parameter values specific to this study are provided in Appendix A, while a full description of the LADDIE model is given in Lambert et al. (2026).

3.2.2. Evaluation Experiments

We evaluate the SFD implementation in LADDIE against the MITgcm simulations for Thwaites described in Section 3.1.1. LADDIE is configured with the same 2013 Thwaites ice-shelf geometry as MITgcm (Figures 1a and 1c) at a comparable horizontal resolution (maximum triangular grid edge length of 200 m, as stated above).

The ambient ocean forcing is taken from the three-dimensional temperature and salinity fields of the MITgcm simulation without SFD. Because the LADDIE mesh differs from the MITgcm grid, the position of the grounding line and ice-shelf base can differ slightly, so LADDIE may require ambient values at locations that are masked in MITgcm (bedrock, grounded ice and ice shelf). We fill these cells with depth-averaged temperature and salinity to obtain complete forcing fields. A Gaussian filter is then applied to the filled three-dimensional fields to remove strong horizontal gradients that could cause numerical instabilities in LADDIE. Alternative interpolation schemes were tested but did not substantively affect the results, while this approach gave the most numerically stable configuration.

We deliberately force LADDIE with these smoothed cavity conditions rather than the open-ocean boundary conditions used to force MITgcm, because the ocean conditions change substantially between the open boundary and the ice-shelf cavity. This ensures that any differences between the models reflect the subglacial discharge representation itself rather than discrepancies in ocean forcing, as our focus is specifically on assessing the SFD implementation rather than LADDIE's overall performance (for which we refer to Lambert et al. (2026)).

The drag coefficient $C_{d,\mathrm{top}}$ in LADDIE is tuned following Lambert et al. (2023) such that the integrated sub-shelf melt flux within the deep grounding-zone region (cropped region shown in Figures 1a and 1c) matches that of the MITgcm simulation without SFD. This calibration yields $C_{d,\mathrm{top}} = 2.5 \times 10^{-3}$. After calibration, SFD forcing is applied along the deep grounding-line segment corresponding to the region used in MITgcm (yellow segment in Figure 1c), using identical flux magnitudes ranging from 0 to 640 m^3 s^{-1} (Table 1). Note that in this setup, 3D cavity-resolving ocean model data is available for calibration; when forcing LADDIE with observations or coarse ice-front ocean model data, calibration is typically performed against satellite-derived melt rates (for example, Lambert et al. (2026)).

21699291, 2026, 12, Downloaded from https://agupubs.onlinelibrary.wiley.com/doi/10.1029/2026JC024641 by British Antarctic Survey, Wiley Online Library on [27/11/2026]. See the Terms and Conditions (https://onlinelibrary.wiley.com/terms-and-conditions) on Wiley Online Library for rules of use; OA articles are governed by the applicable Creative Commons License

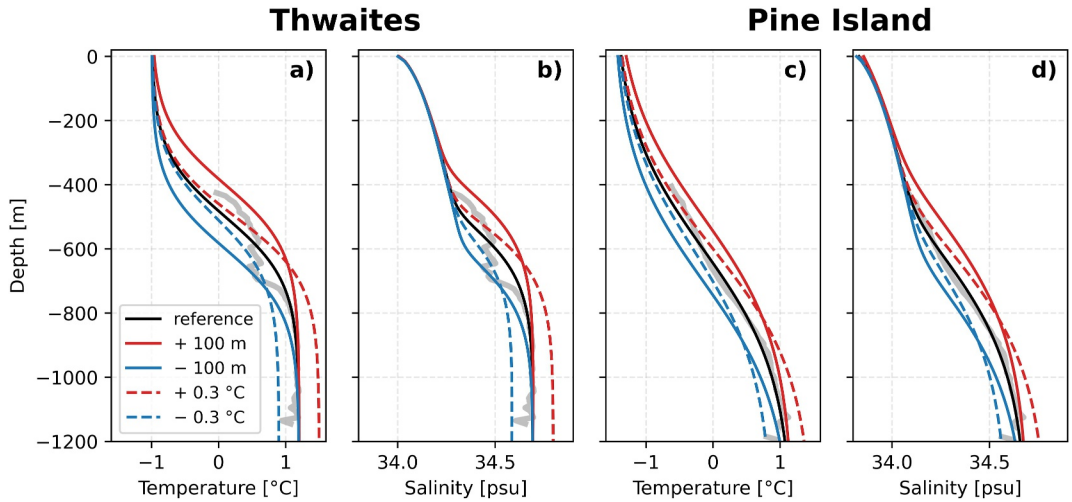


Figure 3. Idealized reference temperature and salinity profiles (black) for Thwaites (a, b) and Pine Island (c, d), and their perturbations used in the ambient ocean sensitivity experiments: thermocline and halocline shifted by ±100 m (solid), and deep-water temperature and salinity changed by ±0.3°C and ±0.1 psu (dashed). The thick gray line shows the horizontally averaged MITgcm temperature and salinity over the regions in Figure 1b (Pine Island) and Figure 1c (Thwaites) on which the reference profiles are based.

3.2.3. Sensitivity Experiments

For both Thwaites and Pine Island, we perform two sets of sensitivity experiments with LADDIE to investigate how (a) ambient ocean conditions and (b) the SFD release location affect SFD-enhanced melting. In each set, one of these factors is perturbed while the other is kept at its reference. We first describe the settings shared by all experiments, and then, for each set, the reference state and the perturbations.

3.2.3.1. Shared Settings

All sensitivity experiments use fixed geometries per ice shelf: the 2013 geometry for Thwaites (Figures 1a and 1c, same as for the evaluation experiments) and the 2023 geometry for Pine Island (Figures 1a and 1b), both consistent with the respective MITgcm simulations (Sections 3.1.1 and 3.1.2). The drag coefficient $C_{d,\mathrm{top}}$ calibrated for Thwaites in the evaluation experiments is retained across all simulations. The same value is applied to Pine Island, where it yields good agreement with the MITgcm simulation without SFD (Figure S1 in Supporting Information S1), making recalibration unnecessary, consistent with recent studies showing that a single calibration performs relatively well at pan-Antarctic scales (Lambert et al., 2026; Reese et al., 2026). Both sets of sensitivity experiments explore a range of SFD flux strengths (Table 1) to assess how melt rates scale with freshwater input. Compared with Thwaites, the Pine Island experiments include one additional flux strength, 50 $m^3\ s^{-1}$, because it corresponds to the estimated present-day steady-state discharge of Pine Island (Ehrenfeucht et al., 2025).

3.2.3.2. Ambient Ocean Conditions

The sensitivity experiments use laterally uniform, idealized temperature and salinity profiles, applied below the meltwater layer. For each ice shelf, we construct a reference profile in which temperature follows a hyperbolic tangent function (Jesse et al., 2025; Lambert & Burgard, 2025), and salinity follows the same form below 400 m, with the halocline at the thermocline depth. To maintain numerical stability in LADDIE, we must ensure a sufficient background stratification in the upper water column. We apply a quadratic depth dependence in salinity over the upper layer, which is qualitatively in line with the strong stratification observed offshore in Pine Island Bay (Dutrieux et al., 2014). The parameters of the reference profiles are chosen to match, as closely as possible, the horizontally averaged deep-cavity conditions in the MITgcm simulations without SFD (gray lines in Figure 3) over the regions of interest, that is, the areas shown in the insets of Figures 1b and 1c. The reference profiles are independent of the SFD forcing: by forcing LADDIE with cavity conditions from the MITgcm simulations without SFD, any SFD-enhanced melt in LADDIE arises from the SFD release itself and not from SFD-induced changes in the ambient conditions.

21699291, 2026, 12, Downloaded from https://agupubs.onlinelibrary.wiley.com/doi/10.1029/2026JC024641 by British Antarctic Survey, Wiley Online Library on [27/11/2026]. See the Terms and Conditions (https://onlinelibrary.wiley.com/terms-and-conditions) on Wiley Online Library for rules of use; OA articles are governed by the applicable Creative Commons License

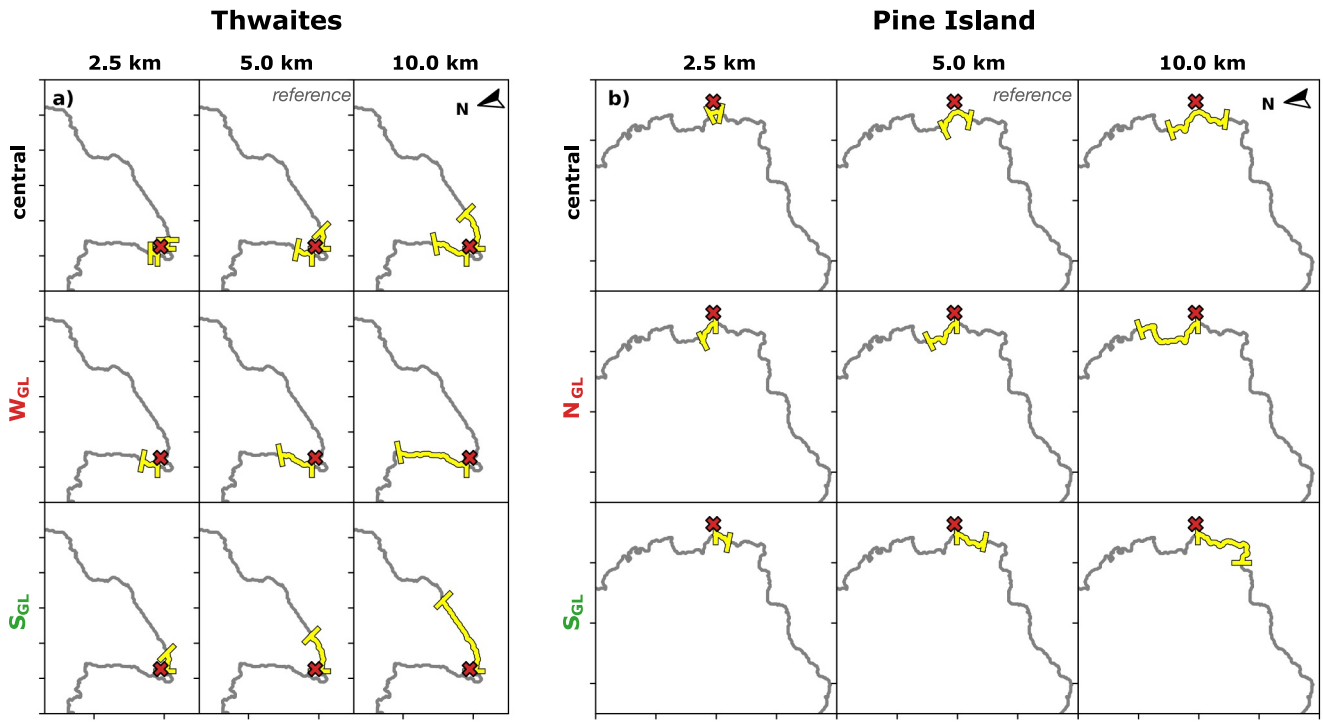


Figure 4. SFD release segments along the grounding lines of Thwaites (a) and Pine Island (b). The yellow lines indicate the prescribed release segments. Labels on the left of each panel denote the segment name, and labels on the top indicate the release width. The red crosses mark the estimated location of subglacial discharge from Ehrenfeucht et al. (2025). The reference release is the central segment with a width of 5 km.

For Thwaites, the reference profile features a sharper thermocline and halocline centered at 500 m depth, with a surface layer at −1.0 °C and 34.0 psu and a deep layer at 1.2°C and 34.7 psu (Figures 3a and 3b). For Pine Island, the deep-layer properties are identical, but the surface layer is at −1.4°C and 33.8 psu, and the thermocline and halocline are more gradual and centered at 600 m (Figures 3c and 3d). This difference arises within the cavities: while MITgcm simulates similar steepness of the thermocline and halocline at the two ice shelf fronts, the simulated cavity circulation modifies the temperature and salinity properties differently as the water enters the respective cavities.

In the ambient ocean sensitivity experiments, we shift the thermocline and halocline up or down by 100 m, and we increase or decrease the deep-water temperature and salinity together by 0.3°C and 0.1 psu (warmer and saltier, or colder and fresher), with ranges that fall within present-day variability (Dutrieux et al., 2014; Webber et al., 2017; Wild et al., 2025) and possible future warming over a 50-year time scale (Naughten et al., 2023). These ambient ocean sensitivity experiments use the reference SFD release location (yellow segments in Figures 1b and 1c; see next paragraph).

3.2.3.3. SFD Release Location

To assess the influence of the SFD release location on SFD-enhanced melting, we vary both the lateral location and width of the SFD release region, while keeping the ambient ocean profiles constant at the reference profiles. For Thwaites, the reference release location (yellow segment in Figure 1c) follows Gourmelen et al. (2025) and has a width of about 5 km. For Pine Island, we use the same width and derive the location from subglacial hydrology modeling constrained by ice sheet geometry from BedMachine v3.2 (Ehrenfeucht et al., 2025; Morlighem et al., 2020) (Figure 1b). Around these reference locations, we test narrower (∼2.5 km) and wider (∼10 km) release bands and lateral shifts relative to the reference (Figure 4). The widths (2.5, 5.0, and 10.0 km) refer to the effective channel width, defined as selecting all grounding-line cells within a fixed lateral distance of the reference release location, assuming a straight grounding line. The channel width thus corresponds to a simplified representation of the release region, rather than the actual along-grounding-line extent, which may be larger due to grounding-line curvature.

21699291, 2026, 12, Downloaded from https://agupubs.onlinelibrary.wiley.com/doi/10.1029/2026JC024641 by British Antarctic Survey, Wiley Online Library on [27/11/2026]. See the Terms and Conditions (https://onlinelibrary.wiley.com/terms-and-conditions) on Wiley Online Library for rules of use; OA articles are governed by the applicable Creative Commons License

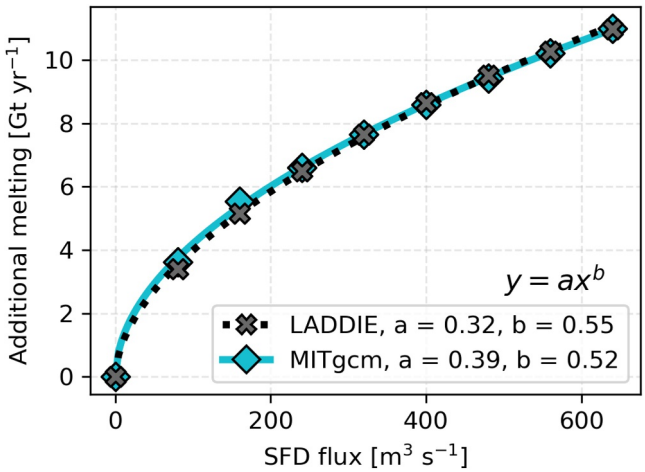


Figure 5. Scaling of additional integrated melt from SFD for Thwaites ice shelf, defined relative to the reference simulation (SFD flux = 0 m^3 s^{-1}). Results from individual model simulations are shown as gray crosses for LADDIE and cyan diamonds for MITgcm. A power-law fit ($y = ax^b$, with y the additional melting and x the SFD flux) is overlaid, with fitted parameter values provided in the legend.

The different ocean and SFD settings of all LADDIE experiments are summarized in Table 1.

AI tools, specifically Claude and ChatGPT, were used to enhance the readability of specific paragraphs during manuscript preparation. All suggestions were critically reviewed and edited as necessary. The authors take full responsibility for the content of the final publication.

4. Model Evaluation

Following calibration, LADDIE reproduces the integrated melt rate over the deep grounding zone of Thwaites (region in Figure 1c), yielding 18.17 Gt yr^{-1}, in close agreement with MITgcm (18.18 Gt yr^{-1}), which here is treated as the reference benchmark in a perfect-model comparison framework. We restrict this comparison to the deep grounding zone because the crevassed regions downstream are represented differently in the two models, which affects the ice-shelf-integrated melt rates and complicates a direct comparison of integrated values. As SFD has no robust effect on melt outside this region, our analysis concentrates on the deep grounding zone.

The increase in melt with stronger SFD flux within the deeper region scales similarly in both models (Figure 5), with power-law exponents of 0.55 for LADDIE and 0.52 for MITgcm. These values are slightly lower than the exponent of 2/3 reported by Vaňková et al. (2025b), who examined the same relationship for channelized discharge in an idealized ice-shelf configuration. While integrated melt rates provide a useful bulk comparison, they do not reveal spatial variations in melting beneath the ice shelf, which are critical for understanding the underlying processes. We therefore examine the spatial patterns of melt in both models.

In the reference state without SFD, LADDIE reproduces most of the spatial variability in melt rates as simulated by MITgcm (Figures 6a and 7a). LADDIE captures the relatively low melt rates within the inverted basal depression (shallow ice; indicated in Figure 6d), consistent with MITgcm. These low values arise from the accumulation of a 'pond' of slow-moving meltwater in this region, which suppresses friction velocity and lowers thermal driving in both models (Figures 6b, 6c, 7b, and 7c). Because LADDIE and MITgcm define the layer over which thermal driving and friction velocity are computed differently (a fixed depth range in MITgcm vs. the dynamic mixed layer in LADDIE; Section 3.2.1), we focus on spatial patterns and relative changes of these quantities rather than absolute values.

Both models simulate the highest melt rates in the deeper part of the ice shelf, but at different locations: LADDIE simulates peak melt along the southern grounding line (S_{GL}, indicated in Figure 6a), whereas MITgcm simulates peak melt along the western grounding line (W_{GL}, indicated in Figure 7a). In MITgcm, the elevated melt rates along the W_{GL} are associated with strong friction velocities in this region (Figure 7c). Here, the near-ice flow is supported by a cyclonic barotropic flow along the f/H contours that enhances recirculation along the W_{GL} (Figure 7d and Figure S2 in Supporting Information S1). In contrast, LADDIE does not include a barotropic flow component. The friction velocity is therefore driven entirely by buoyancy and follows the ice-shelf draft along the S_{GL}, enhancing melt rates there (Figures 6a and 6c). The difference in the location of peak melt between the models thus likely reflects the barotropic circulation, which modulates the buoyancy-driven flow in MITgcm but is absent in LADDIE.

The difference between the models may also be influenced by the thickness of the near-ice layer used to diagnose the flow. In MITgcm, near-ice velocities are evaluated over a 10 m thick layer below the ice base, whereas the corresponding boundary layer in LADDIE is substantially thinner along the W_{GL} and S_{GL} (Figure S3 in Supporting Information S1). The MITgcm friction velocities may therefore reflect a greater contribution from the underlying circulation, rather than solely the boundary flow. Despite these differences, both models agree well in integrated melt rates and capture broadly similar spatial patterns.

Introducing an SFD flux of 80 m^3 s^{-1} over the regions indicated in Figure 1c leads to a strong increase in sub-shelf melting along the S_{GL} in both models (Figures 6e and 7e). In LADDIE, the additional freshwater strengthens the

21699291, 2026, 12, Downloaded from https://agupubs.onlinelibrary.wiley.com/doi/10.1029/2026JC024641 by British Antarctic Survey, Wiley Online Library on [27/11/2026]. See the Terms and Conditions (https://onlinelibrary.wiley.com/terms-and-conditions) on Wiley Online Library for rules of use; OA articles are governed by the applicable Creative Commons License

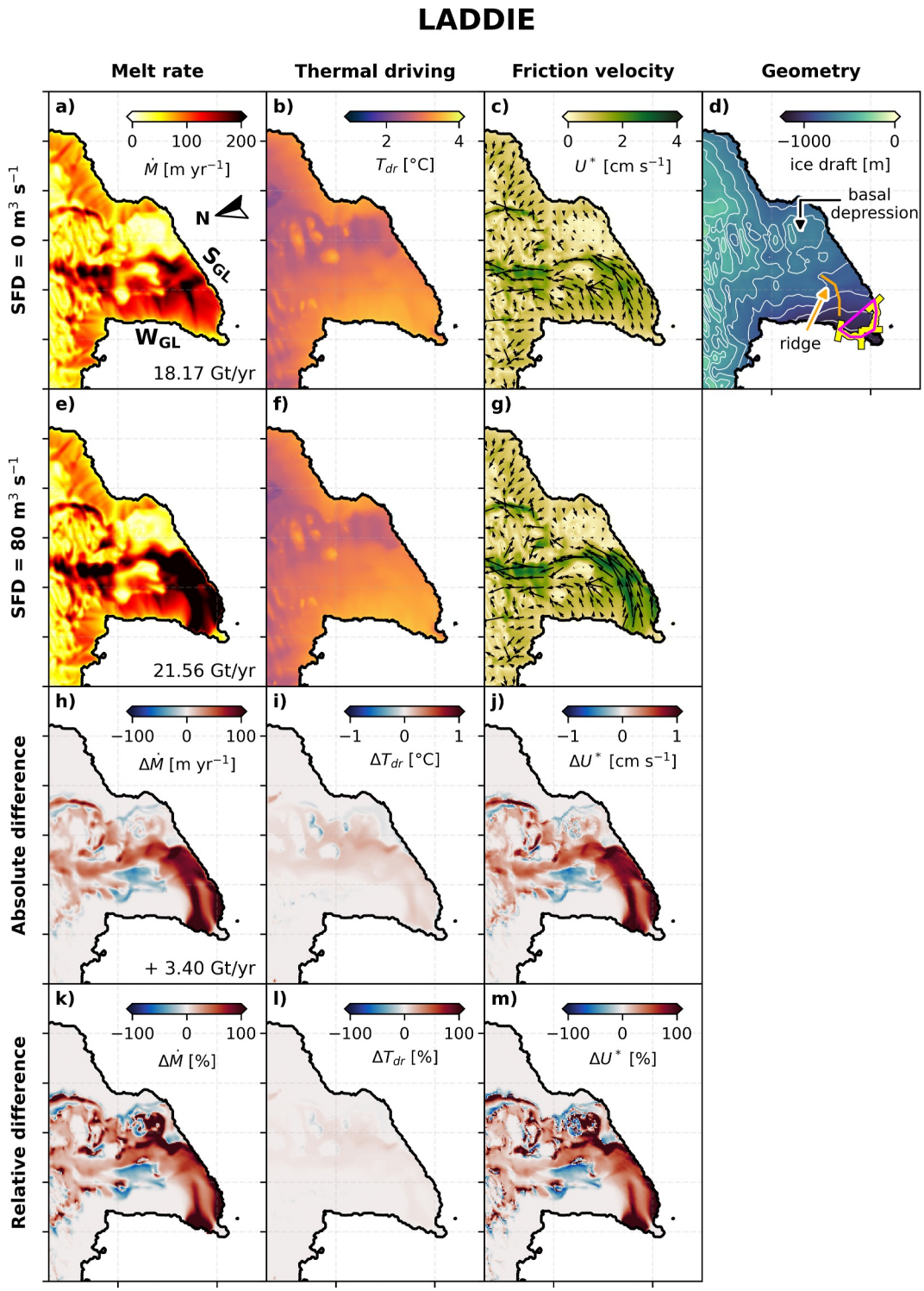


Figure 6. LADDIE simulations: Melt rate ($\dot{M}$; first column), thermal driving (T_{dr}; second column) and friction velocity (U^*; third column) from the reference simulation without subglacial freshwater discharge (SFD; first row) and from the simulation with an SFD flux of 80 m^3 s^{-1} (second row). The third row shows the absolute differences (SFD minus reference) and the fourth row shows the relative differences (in % of the reference). Numbers in panels a, e and h give the ice-shelf-integrated melt (Gt yr^{-1}) and its change. Arrows in c and g show the direction of the friction velocity. Panel d shows the ice-shelf draft (colormap and contours at 100 m spacing) and the SFD release locations in LADDIE (yellow) and MITgcm (magenta), with two geometric features highlighted: a basal depression and a ridge of locally thicker ice (orange).

21699291, 2026, 12, Downloaded from https://agupubs.onlinelibrary.wiley.com/doi/10.1029/2026JC024641 by British Antarctic Survey, Wiley Online Library on [27/11/2026]. See the Terms and Conditions (https://onlinelibrary.wiley.com/terms-and-conditions) on Wiley Online Library for rules of use; OA articles are governed by the applicable Creative Commons License

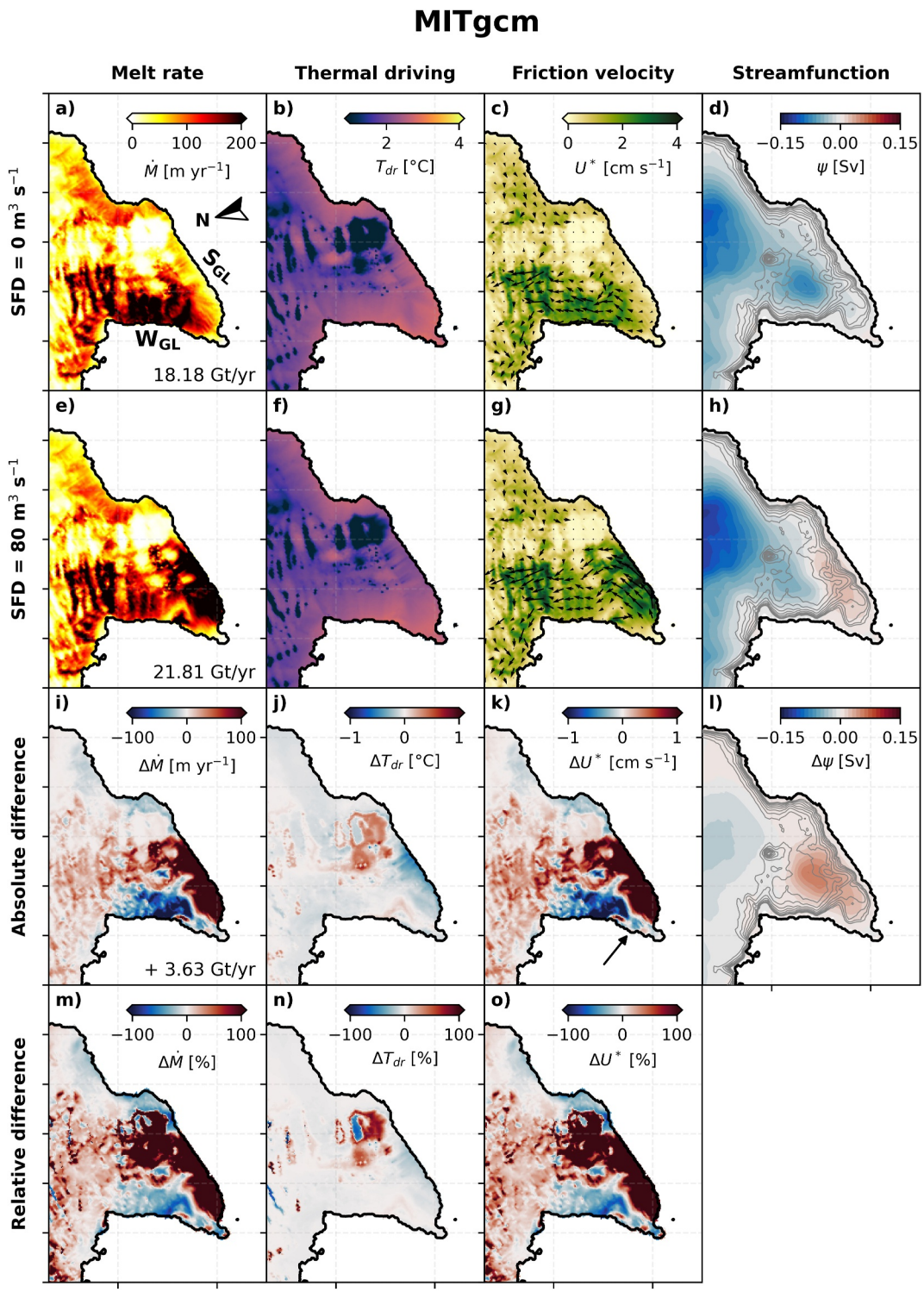


Figure 7. MITgcm simulations: Melt rate ($\dot{M}$; first column), thermal driving (T_{dr}; second column) and friction velocity (U^*; third column) from the reference simulation without subglacial freshwater discharge (SFD; first row) and from the simulation with an SFD flux of 80 $\mathrm{m^3\ s^{-1}}$ (second row). The third row shows the absolute differences (SFD minus reference) and the fourth row shows the relative differences (in % of the reference). Numbers in panels a, e and i give the ice-shelf-integrated melt ($\mathrm{Gt\ yr^{-1}}$) and its change. Arrows in c and g show the direction of the friction velocity. The fourth column shows the barotropic streamfunction (ψ), with negative values indicating clockwise circulation. Gray contours show lines of constant f/H, where f is the Coriolis parameter and H is the water column thickness.

21699291, 2026, 12, Downloaded from https://agupubs.onlinelibrary.wiley.com/doi/10.1029/2026JC024641 by British Antarctic Survey, Wiley Online Library on [27/11/2026]. See the Terms and Conditions (https://onlinelibrary.wiley.com/terms-and-conditions) on Wiley Online Library for rules of use; OA articles are governed by the applicable Creative Commons License

21699291, 2026, 12, Downloaded from https://agupubs.onlinelibrary.wiley.com/doi/10.1029/2026JC024641 by British Antarctic Survey, Wiley Online Library on [27/11/2026]. See the Terms and Conditions (https://onlinelibrary.wiley.com/terms-and-conditions) on Wiley Online Library for rules of use; OA articles are governed by the applicable Creative Commons License

buoyancy-driven flow along the S_{GL} (Figure 6g), increasing melt rates locally and further downstream (Figure 6h). In MITgcm, the freshwater input disrupts the strong cyclonic circulation (Figures 7h and 7l and Figure S2 in Supporting Information S1), reducing friction velocities and, consequently, melt rates along the W_{GL} relative to the SFD = 0 m^3 s^{-1} case (Figures 7i and 7k). This suppression also extends into the western part of the release region (arrow in Figure 7k). Along the S_{GL}, the vertically averaged flow now aligns with the buoyancy-driven flow, which is directed toward shallower ice draft (Figure 6d and Figure S2 in Supporting Information S1). This allows friction velocities to increase, leading to a substantial increase in melt rates along the S_{GL} (Figures 7i and 7k).

Relative changes in thermal driving induced by SFD are small compared to the relative changes in friction velocity, whose spatial pattern closely matches that of the relative melt increase, in both LADDIE and MITgcm (bottom row of Figures 6 and 7). This shows that the models agree on the primary mechanism by which SFD enhances melting: an increase in friction velocity, rather than a change in thermal forcing. The route to this increase differs: in LADDIE, the freshwater source directly strengthens the buoyancy-driven flow that already dominates the friction velocity without SFD, whereas in MITgcm it rearranges the barotropic circulation, so that the buoyancy-driven flow along the upslope ice-draft gradient is no longer opposed and comes to dominate the friction velocity.

Overall, for SFD = 80 m^3 s^{-1}, MITgcm and LADDIE agree well in the spatial pattern of melt, with consistently higher melt along the S_{GL}. In both models, increasing the SFD flux amplifies this pattern without substantially altering it, so the agreement extends to stronger fluxes (see Figure S4 in Supporting Information S1 for the strongest case, SFD = 640 m^3 s^{-1}).

The combined agreement between LADDIE and MITgcm in both scaling behavior and spatial melt patterns once SFD is included demonstrates that, for the Thwaites setup tested here, LADDIE provides a credible representation of SFD-enhanced sub-shelf melting. Importantly, this is achieved at substantially reduced computational cost: the simulations shown require only 20 CPUs for LADDIE to reach steady state in 10 model days, compared to 10,260 CPUs for MITgcm to reach steady state in 6 model months. Together with the agreement in the underlying mechanisms, this makes LADDIE an efficient tool for exploring a broader parameter space. In the following sections, we use LADDIE to investigate the sensitivity of SFD-driven melt to variations in ambient ocean conditions and freshwater release locations for the Thwaites and Pine Island ice shelves.

5. Sensitivity of SFD-Enhanced Melt to Ambient Ocean Conditions

Across the explored ambient ocean states, the absolute increase in sub-shelf melting induced by SFD varies only moderately, and is slightly larger under warmer conditions than under colder ones. However, owing to lower background melt rates in a colder state, the relative SFD-induced increase in melt is greater under colder conditions.

For Thwaites, the absolute increase in integrated melt flux associated with SFD varies only between 3.25 and 3.48 Gt yr^{-1} across the explored ocean states (Figures 8a–8e). This limited sensitivity arises because the reference thermocline and halocline are relatively shallow, such that the deep cavity regions influenced by SFD remain within the warm, saline deep-water layer even when the thermocline and halocline depth varies. Consequently, shoaling or deepening of the thermocline and halocline has little effect on the temperature and salinity in regions where the strongest SFD-driven enhanced melting occurs (Figures 8b and 8c). Variations in deep-water temperature and salinity only moderately affect the absolute magnitude of the melt enhancement, primarily by altering the density gradient between the meltwater layer and the ambient ocean, which controls the friction velocity. As a result, warmer and saltier conditions increase the additional melt flux, whereas cooler and fresher conditions reduce it (Figures 8d and 8e).

For Pine Island, the range of the absolute increase in integrated melt flux is larger, spanning 2.97 to 3.46 Gt yr^{-1} across the explored ocean states (Figures 8f–8j). Compared to Thwaites, the Pine Island ice-shelf base near the grounding line (draft of 800–1,200 m) is closer to the reference thermocline and halocline (Figures 3c and 3d), so variations in thermocline and halocline depth more directly alter the water properties in regions affected by SFD. In particular, a deepening thermocline and halocline introduces colder and fresher water into these regions, reducing the density gradient between the meltwater layer and the surrounding ocean. This weakens the resulting friction velocity and therefore decreases the additional melt flux compared with scenarios with a shallower thermocline and halocline (Figures 8g and 8h). Changes in deep-water properties show a similar response as for Thwaites: warmer and saltier ambient waters enhance the density contrast, leading to stronger friction velocities and larger melt increases (Figures 8i and 8j).

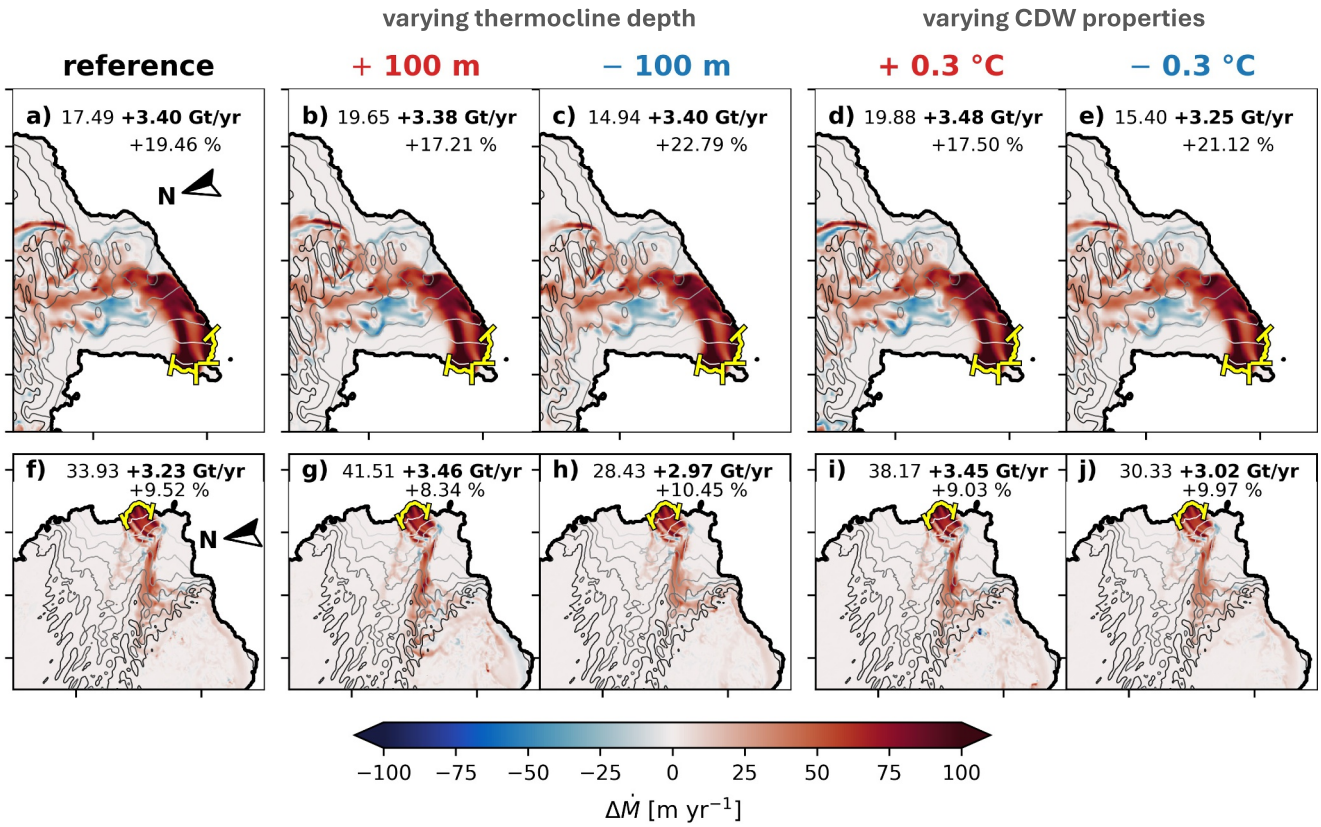


Figure 8. SFD-driven melt anomalies under a range of ambient ocean conditions (e.g., thermocline and halocline depth varied by ±100 m, and deep water properties varied by ±0.3 °C and ±0.1 psu; full profiles shown in Figure 3) for Thwaites with an SFD flux of 80 m^3 s^{-1} (a–e) and Pine Island with an SFD flux of 50 m^3 s^{-1} (f–j). In each panel, the release location is indicated by the yellow segment. For each forcing scenario, the reference melt flux (without SFD) is indicated at the top of each panel, with the corresponding absolute increase in melt flux due to SFD shown in bold. Relative increases in melt (percent change) are also provided.

In general, the absolute increase in melting is slightly larger under warmer and saltier conditions, compared to colder and fresher conditions. More significant differences, however, are found in the relative increases which are strongest in colder fresher conditions. For Thwaites, the relative melt increase ranges from 21.12% to 22.79% in colder and fresher conditions (Figures 8c and 8e), compared to 17.21%–17.50% in warmer and saltier conditions (Figures 8b and 8d). For Pine Island, it ranges from 9.97% to 10.45% in colder and fresher conditions (Figures 8h and 8j), compared to 8.34%–9.03% in warmer and saltier conditions (Figures 8g and 8i). The larger relative contribution of SFD to total melting in colder and fresher scenarios occurs because the baseline melt flux is lower in these colder conditions. This difference is stronger than the absolute differences in melt increase.

Because SFD-induced changes in thermal driving are small, melt-rate variations are governed primarily by SFD-induced changes in friction velocity. In all cases, the introduction of zero-salinity SFD produces a strong and persistent buoyancy contrast relative to the ambient ocean, which consistently enhances friction velocity beneath the ice shelf. Variations in ambient temperature and salinity only weakly modulate this response by slightly altering the density contrast between the meltwater layer and the surrounding ocean, with sensitivity primarily emerging when the ice-shelf base and SFD release region lie closer to the thermocline and halocline. As a result, the friction velocity response is broadly consistent across the considered ocean states, leading to similar spatial patterns and absolute magnitudes of SFD-driven melt enhancement.

6. Sensitivity of SFD-Enhanced Melt to Release Location

We find that the source location of SFD strongly influences the spatial pattern of melt enhancement and, depending on the downstream meltwater pathway, can also affect the increase in integrated melt flux. Meltwater pathways that diverge laterally across the ice base distribute the SFD-induced buoyancy forcing over a larger area,

21699291, 2026, 12, Downloaded from https://agupubs.onlinelibrary.wiley.com/doi/10.1029/2026JC024641 by British Antarctic Survey, Wiley Online Library on [27/11/2026]. See the Terms and Conditions (https://onlinelibrary.wiley.com/terms-and-conditions) on Wiley Online Library for rules of use; OA articles are governed by the applicable Creative Commons License

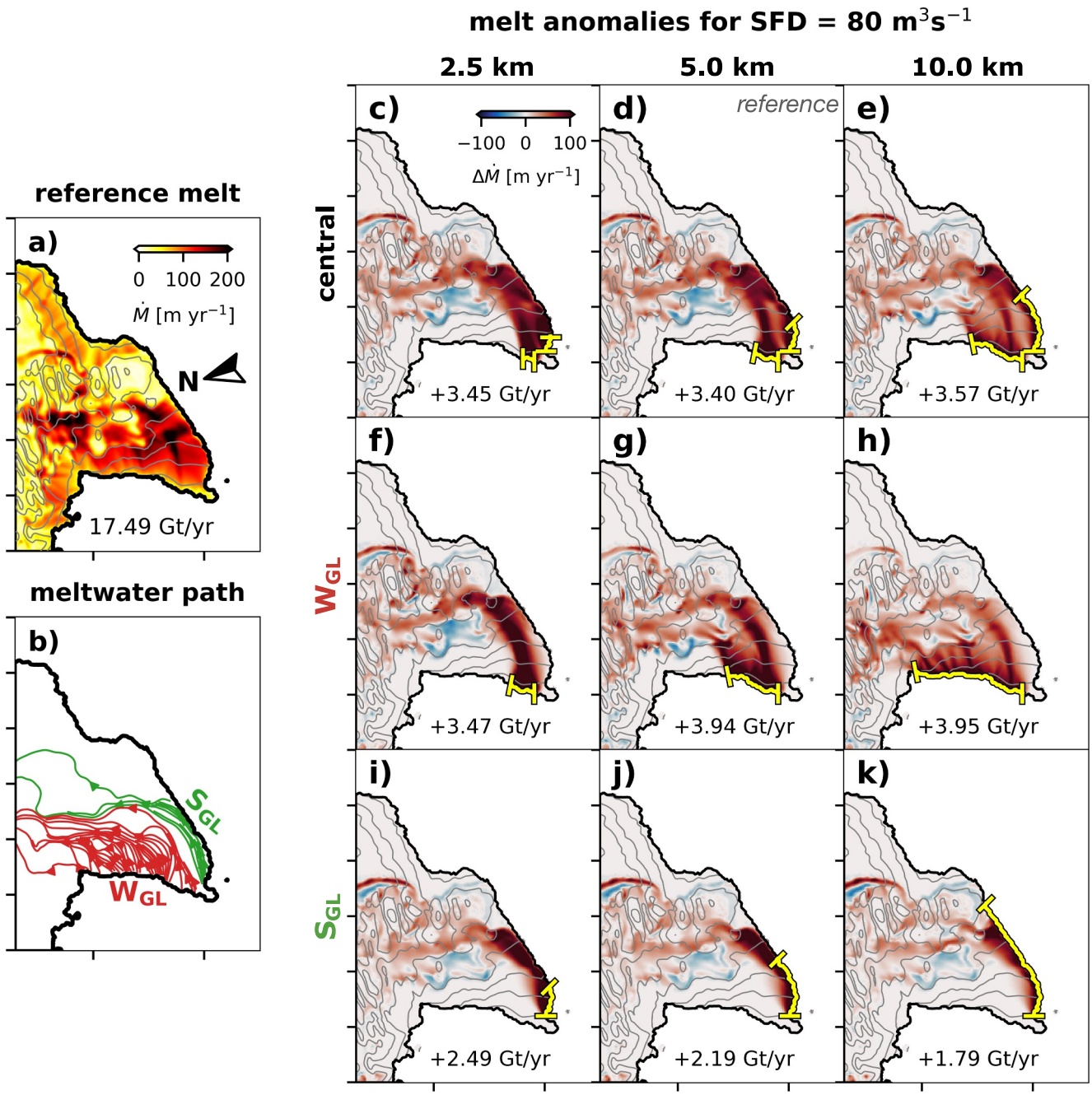


Figure 9. Melt anomalies at Thwaites resulting from SFD of 80 m^3 s^{-1}, for different release locations indicated by the yellow segment in each panel (c–k). The top row shows the central release, the middle row release along the western grounding line (W_{GL}), and the bottom row release along the southern grounding line (S_{GL}). The columns correspond to different widths of the release region. Melt rates for the reference case are shown in (a). Draft contours are overlaid in all panels except for (b). In (b), meltwater flow streamlines are shown for the reference simulation, with streamlines separated by origin at either the W_{GL} (red) or the S_{GL} (green).

resulting in a more efficient enhancement of melt rates, whereas laterally-convergent pathways confine the buoyancy forcing and limit the spatial extent of the melt response.

For Thwaites, varying the width of the discharge region around the reference release location leads to a similar increase in integrated melt, ranging between 3.40 and 3.57 Gt yr^{-1}, but substantially alters the spatial distribution of enhanced melting (Figures 9c–9e). A narrow discharge concentrates the buoyancy input, producing strong increases in friction velocities and thus melt rates along a confined pathway following the S_{GL} (Figures 9c and 9d). In contrast, distributing the freshwater input over a broader region results in weaker local buoyancy enhancement

21699291, 2026, 12, Downloaded from https://agupubs.onlinelibrary.wiley.com/doi/10.1029/2026JC024641 by British Antarctic Survey, Wiley Online Library on [27/11/2026]. See the Terms and Conditions (https://onlinelibrary.wiley.com/terms-and-conditions) on Wiley Online Library for rules of use; OA articles are governed by the applicable Creative Commons License

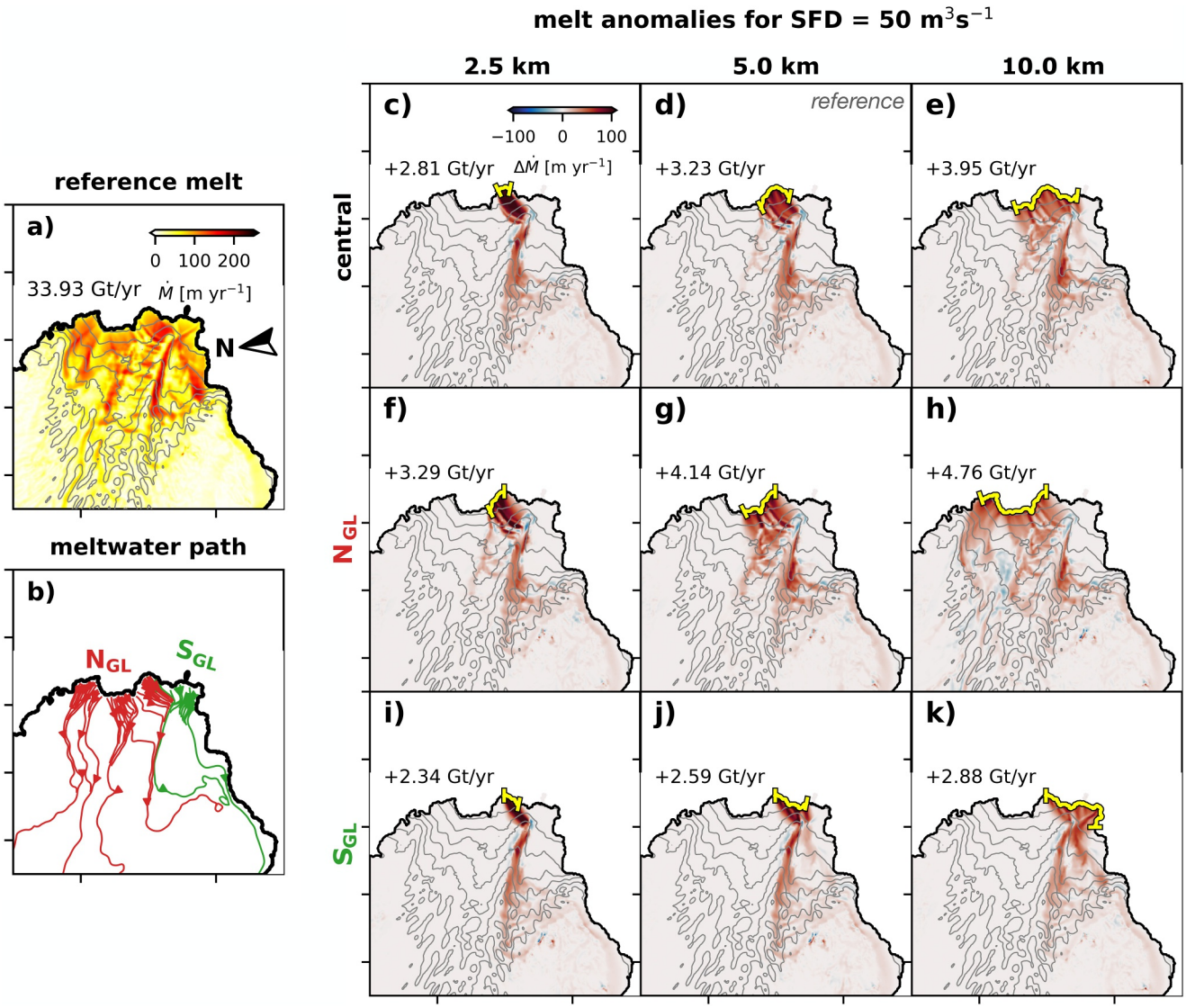


Figure 10. Melt anomalies at Pine Island resulting from SFD of 50 m^3 s^{-1}, for different release locations indicated by the yellow segment in each panel (c–k). The top row shows the central release, the middle row release along the northern grounding line (N_{GL}), and the bottom row release along the southern grounding line (S_{GL}). The columns correspond to different widths of the release region. Melt rates for the reference case are shown in (a). Draft contours are overlaid in all panels except for (b). In (b), meltwater flow streamlines are shown for the reference simulation, with streamlines separated by origin at either the N_{GL} (red) or the S_{GL} (green).

and therefore smaller increases in friction velocities and melt rates, while affecting a larger area of the ice-shelf base (Figure 9e).

Distributing the SFD along either the S_{GL} or W_{GL} demonstrates that the meltwater pathway, determined by ice-shelf geometry, governs the magnitude of additional melting. Freshwater released along the S_{GL} results in a smaller increase in integrated melt than discharge along the W_{GL}. Flow pathways originating near the S_{GL} lie along the right-hand side of a minor ridge in the draft geometry and are more laterally confined (Figures 6d and 9b), which limits lateral spreading of the meltwater flow and concentrates the buoyancy forcing along a narrower, more convergent flow path (Figures 9i–9k). In contrast, discharge along the W_{GL} encounters a more divergent meltwater pathway (Figure 9b), causing the buoyancy increases in this region to spread laterally, thereby producing stronger friction velocities and melting over a larger area (Figures 9f–9h). This more divergent meltwater flow originating at the W_{GL} (Figures 9f–9h) results in a greater integrated melt response than the more convergent flow originating at the S_{GL} (Figures 9i–9k).

21699291, 2026, 12, Downloaded from https://agupubs.onlinelibrary.wiley.com/doi/10.1029/2026JC024641 by British Antarctic Survey, Wiley Online Library on [27/11/2026]. See the Terms and Conditions (https://onlinelibrary.wiley.com/terms-and-conditions) on Wiley Online Library for rules of use; OA articles are governed by the applicable Creative Commons License

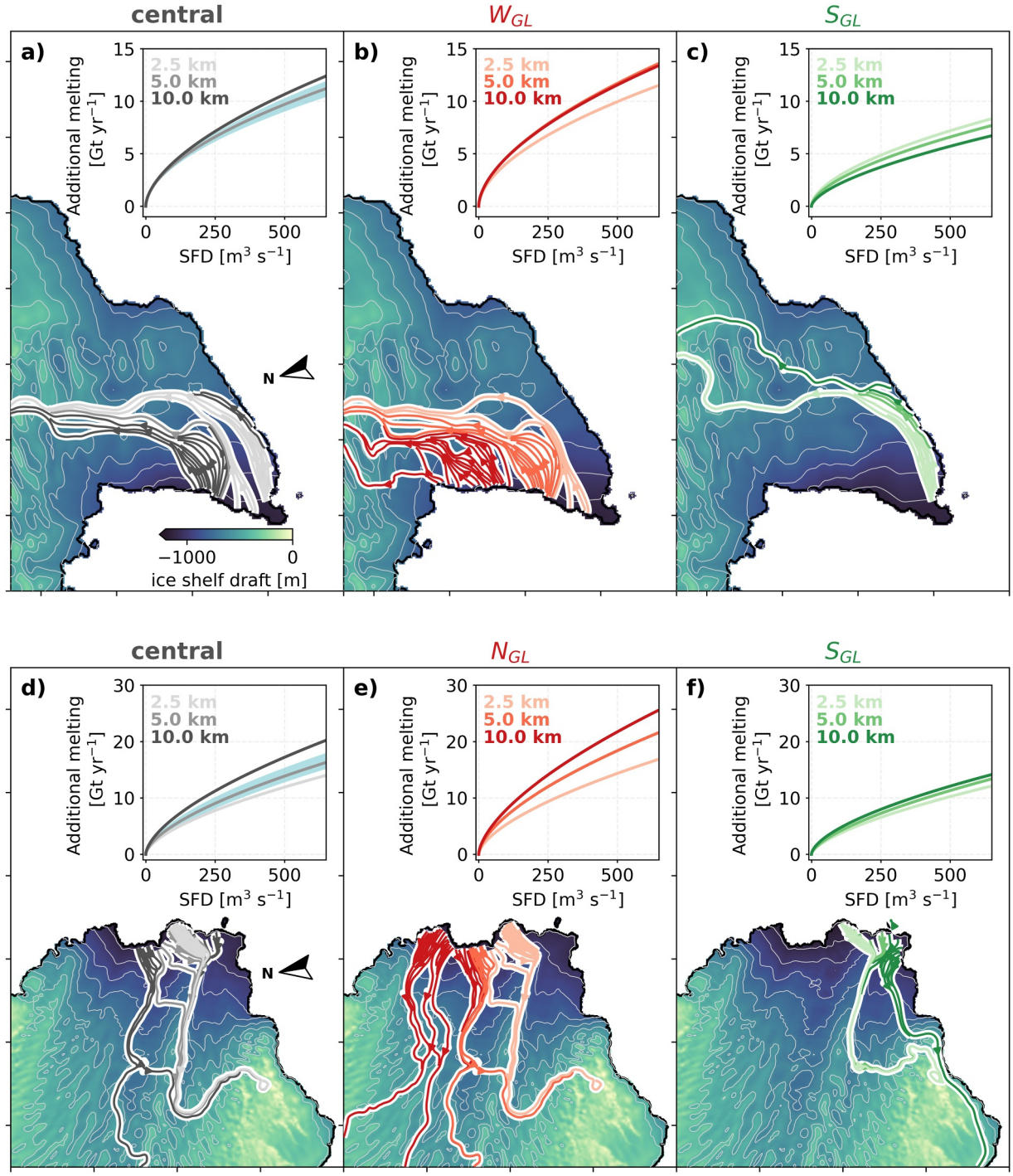


Figure 11. Stream lines of the friction velocity downstream of the subglacial discharge release locations, representing the meltwater pathways for Thwaites (upper row) and Pine Island (bottom row). Streamlines are colored by release location. In each panel, the narrowest release is plotted on top and overlaps with the wider releases. The background shows ice draft (color) and draft contours (gray lines). Insets show how the additional melt scales with the applied SFD flux for each release location. Blue shading in the insets of panels (a) and (d) indicates the range of this scaling across simulations with varying ambient ocean conditions.

For the S_{GL} release location, widening the source systematically reduces the sensitivity of integrated melt to SFD (Figures 9i–9k). Here, the wider release additionally spills into more convergent flow pathways that feed into the same pathways already influenced by the narrow release. Consequently, a part of the buoyancy introduced by SFD is added to regions where the flow converges, making it less effective at increasing melt. This suggests that

21699291, 2026, 12, Downloaded from https://agupubs.onlinelibrary.wiley.com/doi/10.1029/2026JC024641 by British Antarctic Survey, Wiley Online Library on [27/11/2026]. See the Terms and Conditions (https://onlinelibrary.wiley.com/terms-and-conditions) on Wiley Online Library for rules of use; OA articles are governed by the applicable Creative Commons License

Table 2
Power-Law Fit Coefficients for the Relationship Between Additional Melting and Subglacial Freshwater Discharge (SFD)

	Thwaites		Pine Island	
	a	*b*	*a*	*b*
2.5 km	0.31	0.55	0.26	0.62
5.0 km	0.31	0.55	0.30	0.62
10.0 km	0.29	0.58	0.37	0.62
2.5 km–W_{GL}, N_{GL}	0.31	0.56	0.31	0.62
5.0 km–W_{GL}, N_{GL}	0.33	0.57	0.40	0.62
10.0 km–W_{GL}, N_{GL}	0.34	0.57	0.45	0.63
2.5 km–S_{GL}	0.21	0.57	0.19	0.64
5.0 km–S_{GL}	0.17	0.59	0.21	0.64
10.0 km–S_{GL}	0.12	0.62	0.29	0.60
5.0 km$_{+100}$	0.32	0.55	0.35	0.60
5.0 km$_{-100}$	0.30	0.56	0.23	0.65
5.0 km$_{+03C}$	0.30	0.57	0.35	0.61
5.0 km$_{-03C}$	0.31	0.54	0.26	0.63

Note. Expressed as $y = ax^b$, where y is the additional melt flux (Gt yr^{-1}) integrated over the area of interest for the respective ice shelf (Thwaites: Figure 1c, or Pine Island: Figure 1b) and x is the SFD flux (m^3 s^{-1}). The width labels (2.5, 5.0, and 10.0 km) indicate the width of the SFD release region. W_{GL}, N_{GL}, and S_{GL} denote the western, northern, and southern grounding-line regions, respectively, as indicated in Figure 4. The (+100) and (−100) cases denote perturbations to the thermocline and halocline depths, respectively, while (+03C) and (−03C) denote changes in deepwater properties, as indicated in Figure 3.

widening the release does not necessarily enhance melt; rather, the melt response depends on the degree of convergence of the affected meltwater pathways.

At Pine Island, increasing the release width around the reference release location leads to an increase in the additional melt flux, from 2.81 Gt yr^{-1} for a release width of 2.5 km to 3.95 Gt yr^{-1} for a release width of 10.0 km (Figures 10c-e). A wider discharge area spreads the freshwater over a larger portion of the ice-shelf base and enhances melt across multiple basal channels that already exhibit high melt rates in the absence of SFD (Figure 10a). The larger integrated melt increase resulting from a more distributed discharge that feeds more divergent meltwater pathways indicates that the effect of increased spatial extent dominates over the more concentrated buoyancy forcing.

Release along the N_{GL} shows a strong sensitivity of additional melt flux to the release width, with the additional melt flux increasing from 3.29 Gt yr^{-1} for a release width of 2.5 km to 4.76 Gt yr^{-1} for a release width of 10.0 km (Figures 10f–10h). In contrast, releasing freshwater along the S_{GL} results in a more modest increase in additional melt with release width, ranging from 2.34 to 2.88 Gt yr^{-1} (Figures 10i–10k). Similar to Thwaites, this difference is reflected by the meltwater pathways governed by the downstream geometry. Discharge along the N_{GL} encounters a more divergent meltwater pathway, allowing the buoyancy anomaly to spread across multiple parts of the deeper grounding-zone cavity and propagate through the basal channel system (red area in Figure 10b). In contrast, meltwater flow originating near the S_{GL} follows a more convergent pathway, which confines the buoyant plume and limits the spatial extent of melt enhancement, concentrating the additional melting primarily within a single channel (green area in Figure 10b).

For both ice shelves, we find a sub-linear power-law scaling (i.e., exponent smaller than one) of additional melt with increasing SFD. The sensitivity of melt to SFD is stronger for more divergent meltwater pathways than for more convergent ones. The power-law relationship is robust across simulations, with exponents ranging from 0.54 to 0.62 for Thwaites and from 0.60 to 0.65 for Pine Island (Table 2). The sensitivity to the downstream meltwater pathway (i.e., convergent vs. divergent) is primarily represented by the prefactor a. For Thwaites, a ranges from 0.12 to 0.21 for S_{GL} (convergent; Figure 11c) and from 0.31 to 0.34 for W_{GL} (divergent; Figure 11b). For Pine Island, a ranges from 0.19 to 0.29 for S_{GL} (convergent; Figure 11f) and from 0.31 to 0.45 for N_{GL} (divergent; Figure 11e).

21699291, 2026, 12, Downloaded from https://agupubs.onlinelibrary.wiley.com/doi/10.1029/2026JC024641 by British Antarctic Survey, Wiley Online Library on [27/11/2026]. See the Terms and Conditions (https://onlinelibrary.wiley.com/terms-and-conditions) on Wiley Online Library for rules of use; OA articles are governed by the applicable Creative Commons License

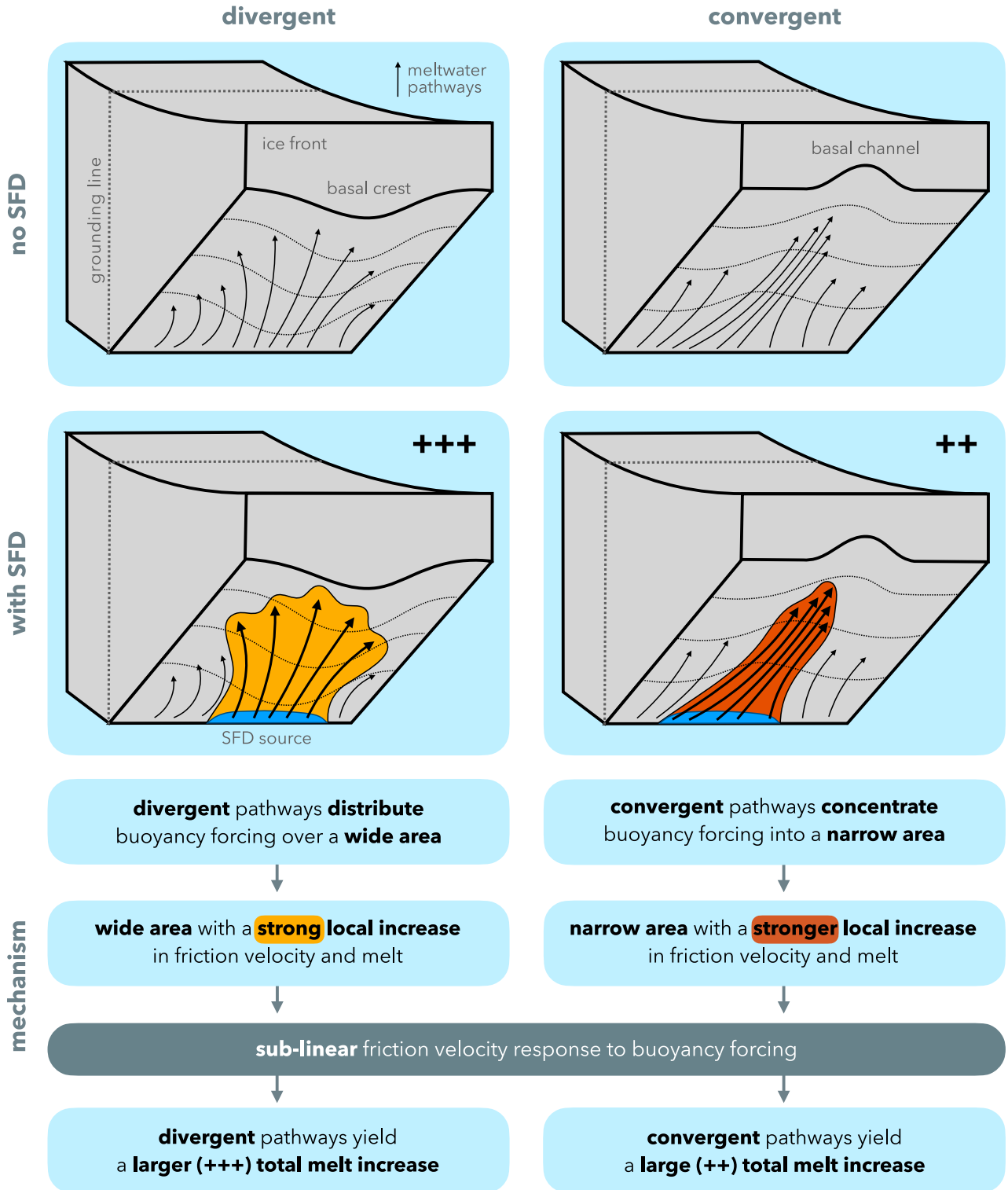


Figure 12. Schematic summarizing how the divergence of meltwater pathways modulates the melt response to subglacial freshwater discharge (SFD). Pathways can be divergent (e.g., over a basal crest; left) or convergent (e.g., in a basal channel; right). SFD, entering at the source (blue), adds buoyancy and enhances friction velocity and sub-shelf melt along the pathways originating near it (second row; thicker arrows indicate enhanced flow compared to the top row without SFD). Divergent pathways distribute this enhancement over a wide area (orange), whereas convergent pathways concentrate it, giving a stronger local melt increase over a narrow area (red). Because friction velocity responds sub-linearly to buoyancy forcing, distributing the forcing is more effective than concentrating it, and the total melt increase is therefore larger for divergent than for convergent pathways (qualitatively indicated by +++ vs. ++).

21699291, 2026, 12, Downloaded from https://agupubs.onlinelibrary.wiley.com/doi/10.1029/2026JC024641 by British Antarctic Survey, Wiley Online Library on [27/11/2026]. See the Terms and Conditions (https://onlinelibrary.wiley.com/terms-and-conditions) on Wiley Online Library for rules of use; OA articles are governed by the applicable Creative Commons License

21699291, 2026, 12, Downloaded from https://agupubs.onlinelibrary.wiley.com/doi/10.1029/2026JC024641 by British Antarctic Survey, Wiley Online Library on [27/11/2026]. See the Terms and Conditions (https://onlinelibrary.wiley.com/terms-and-conditions) on Wiley Online Library for rules of use; OA articles are governed by the applicable Creative Commons License

More broadly, the magnitude of the melt response is controlled by the spatial extent of the meltwater layer influenced by SFD, that is, the area spanned by the dominant meltwater pathways downstream of the release location. Expanding this extent, through shifting to a release location that allows for a more divergent flow configuration, systematically increases the impact of a given SFD flux on the total melt flux (Figure 12). The explored ambient ocean states have only a limited impact on the additional melting relative to the effects of SFD location and release width (blue shading in Figures 11a and 11d).

In general, the increase in a with either increasing discharge width or more divergent meltwater pathways indicates a stronger sensitivity of melt to SFD under more distributed buoyancy forcing. This can be understood within the same physical framework as the sub-linear scaling of melt with increasing SFD flux (insets of Figure 11). Both an increased SFD flux and a downstream meltwater flow convergence act to concentrate buoyancy forcing along meltwater pathways. However, this enhanced buoyancy does not translate into a proportional increase in friction velocity, and therefore not into a proportional increase in melt. The sub-linear friction velocity response reflects a combination of (a) buoyancy–drag scaling in the LADDIE momentum balance (Equation 2–3 in Lambert et al. (2026)), which provides a baseline square-root scaling between friction velocity and buoyancy, and (b) a secondary effect that reshapes the momentum balance through SFD-dependent changes in buoyancy and layer thickness that modify the driving terms. This secondary effect explains the deviation from the square-root scaling implied by buoyancy–drag balance. Furthermore, we find that particularly in convergent meltwater pathways, the meltwater layer thickness initially increases with SFD but approaches a limit as SFD increases toward the maximum tested value. This limits the layer-thickness-dependent driving terms in the momentum balance, thereby reducing the sensitivity of melt to additional SFD compared to divergent pathways.

7. Discussion

While the SFD implementation in LADDIE has only been quantitatively evaluated against MITgcm for the Thwaites ice shelf (Section 4), we observe qualitatively comparable outcomes for Pine Island when comparing to the high-resolution simulations described in Nakayama et al. (2021). We find a similar local melt increase near the release location when applying SFD over a narrow area. A direct comparison of melt patterns is more challenging due to differences in the geometry data set used by Nakayama et al. (2021). Nevertheless, we observe melt amplification within the basal channels, consistent with their results as well as with findings from the Petermann Glacier (Prakash et al., 2025), highlighting the importance of geometry in controlling melt enhancement.

In this study, we focus on the direct effects of SFD on sub-shelf melting and do not explicitly account for potential feedbacks on ambient ocean conditions. Previous work from Vaňková et al. (2025a) indicates that, for Thwaites and Pine Island, such feedbacks have a limited impact on the SFD–melt relationship because the subglacial flux is large relative to ice-shelf area. We find a power-law scaling of SFD-enhanced melt (0.54–0.62 for Thwaites, 0.60–0.65 for Pine Island) that approximately matches the two-thirds power-law scaling reported by Vaňková et al. (2025a), supporting the assumption that neglecting feedbacks on ambient ocean conditions is a reasonable approximation for these ice shelves. The coarser horizontal model resolution (∼12 km) used by Vaňková et al. (2025a) likely does not resolve basal channels that could produce more convergent meltwater pathways, so their reported scaling probably reflects a more divergent-pathway case.

Our results fall within the broader range of sub-linear melt responses to SFD reported in previous studies. These include the two-thirds power-law scaling found in the idealized ice-shelf study by Vaňková et al. (2025b), the one-third power-law scaling reported for tidewater glaciers (Jackson et al., 2022; Xu et al., 2012), and the square-root scaling reported for Greenland's 79 North Glacier (Wekerle et al., 2024). The differences in the power-law scaling exponent that we find between Pine Island and Thwaites, although small, suggest that variations in scaling exponents may depend on the specific ice-shelf geometry.

The sub-linear friction velocity response to SFD partly reflects the buoyancy-drag scaling in LADDIE's momentum balance (Equations 2–3 in Lambert et al. (2026)), where we use a quadratic drag law. Large eddy simulations testing the shear-driven boundary layer assumption show that this law performs well in a highly turbulent regime, whereas in a stratified regime the momentum transfer is weaker than the law predicts (Vreugdenhil & Taylor, 2019). Our setup thus assumes that the meltwater flow is highly turbulent. Future research could test this assumption using boundary-layer formulations that include the role of stratification, and investigate how such alternative drag formulations would influence the scaling of melt with SFD found here.

21699291, 2026, 12, Downloaded from https://agupubs.onlinelibrary.wiley.com/doi/10.1029/2026JC024641 by British Antarctic Survey, Wiley Online Library on [27/11/2026]. See the Terms and Conditions (https://onlinelibrary.wiley.com/terms-and-conditions) on Wiley Online Library for rules of use; OA articles are governed by the applicable Creative Commons License

We find that integrated melt without SFD decreases under ambient cooling and increases under ambient warming (Figure 8), with the warming-driven increase broadly comparable to that expected after 50 years under a 2°C Paris Agreement scenario (Naughten et al. (2023); their Figure 1). Ambient warming thus raises, and cooling lowers, the integrated melt without SFD. In contrast, the additional melting caused by SFD varies only slightly across the explored ocean states (Figure 8). This weak sensitivity to ambient ocean conditions suggests that, in ocean models that do not explicitly resolve ice-shelf cavities or represent SFD-enhanced melting (e.g., non-cavity-resolving ocean components of earth system models), the SFD-induced melt flux may be approximated as a function of the SFD magnitude and release location, both which strongly control it (Figure 11). This approach allows quantification of downstream processes, such as sea-ice formation and circulation (Goldberg et al., 2023), as a function of total meltwater input. Moreover, the weak sensitivity of SFD-induced melting to ambient ocean conditions implies that ice shelves in colder ambient conditions receive a relatively larger fraction of their total melt from SFD. For ice-sheet models, capturing the correct spatial distribution of melt rates thus requires increasingly accurate representation of SFD-enhanced melting under colder conditions. For ocean models, SFD-enhanced melting accounts for a larger share of total melting in colder conditions than in warmer conditions, and therefore a larger share of the freshwater flux entering the ocean model, making its accurate representation similarly important.

Although our conclusions are based on a single snapshot of ice-shelf geometry, the mechanisms governing SFD-enhanced melting identified here are likely robust across a range of geometrical configurations. The key geometrical features controlling whether the flow converges or diverges appear to be the degree of lateral confinement near the grounding zone, for example, by sidewalls or by basal channels that guide the meltwater plumes along the ice-shelf base. A similar effect can be seen in the results by Vaňková et al. (2025b), who studied the idealized MISMIP + domain. They found that releasing SFD at the eastern side of the deeper grounding line led to greater melt enhancement because the plume was able to spread westward along the ice-shelf base, allowing it to diverge and affect a larger area. In contrast, meltwater released further west quickly converged into the western boundary current, limiting its spatial influence and suppressing additional melting. Examining the expected flow patterns beneath different ice-shelf geometries can therefore provide insight into whether SFD-driven melt enhancement is likely to be amplified or suppressed for different release locations.

A similar sensitivity to flow confinement has been identified in studies of buoyant meltwater plumes in Greenland fjords, where distributed discharge enhances lateral spreading of the plume and thus melting (Kimura et al., 2014; Slater et al., 2015). However, these studies consider non-rotating systems with vertical ice faces and therefore do not include Coriolis effects, which have been shown to influence plume pathways in ice-shelf cavities (Vaňková et al., 2025b). Nevertheless, the underlying mechanism remains consistent: reduced confinement, here through distributing SFD over a larger portion of the grounding line, allows greater lateral spreading of the buoyant plume, increasing the area over which enhanced melting can occur.

We note that, overall, the integrated SFD-driven melt increase is small compared to the total sub-shelf melt of the full ice shelf, amounting to around 3 Gt yr^{-1} for both Thwaites and Pine Island, compared to total modeled values of around 43 Gt yr^{-1} and 83 Gt yr^{-1}, respectively. However, the localisation of enhanced melting in dynamically important regions can have a large effect on ice-shelf buttressing and hence ice-sheet volume loss (Reese et al., 2018). For Thwaites, several studies indicate that the deep western trunk grounding zone plays a key role in ice-shelf buttressing (Gudmundsson et al., 2023; Morlighem et al., 2021; Naughten et al., 2023), and hence ice flow is highly sensitive to thinning there. In more spatial detail, Gourmelen et al. (2025) show that the linear sensitivity of volume above flotation to sub-shelf melting is largest along the W_{GL}, implying greater sensitivity to the same amount of melting there than along the S_{GL}. Our results show that SFD release at the W_{GL} enhances melt more strongly along the W_{GL} than release from the S_{GL}. Combined with the higher sensitivity of volume loss along the W_{GL}, this suggests a larger impact on ice-sheet volume loss for western compared to southern release.

At Pine Island, the buttressing potential is strongest close to the deep grounding line and along the shear margins (Gudmundsson et al., 2023; Morlighem et al., 2021; Naughten et al., 2023). While our results do not show a strong increase in melting beneath the shear margins as a result of SFD, we do find enhanced melting near the grounding line. The release location also determines which basal channels experience enhanced melting: concentrated discharge intensifies melt within a single channel, whereas distributed release enhances melt more moderately

across multiple channels. Idealized modeling suggests that high melt rates in basal channels can lead to channel breakthrough (Wearing et al., 2021), and observations indicate that channel incision may promote large-scale fracturing (Alley et al., 2022). Taken together, our results show that SFD-enhanced melting is concentrated in regions of key importance for ice-shelf buttressing, and that the release location can shift or redistribute melt within these dynamically sensitive areas. This suggests that the ice-dynamical response may be sensitive to where subglacial discharge is released, highlighting the need for high-resolution subglacial hydrology models to constrain SFD discharge and for further investigation using fully coupled ice–ocean models.

We emphasize that our simulations are based on a single snapshot of ice-shelf geometry and prescribed SFD locations, whereas in reality both ice-shelf topography and subglacial hydrological pathways evolve dynamically. Recent coupled ice-sheet–hydrology modeling by Pelle et al. (2024) shows that the subglacial drainage network is highly dynamic under changing ice-sheet geometry, with new channels emerging and SFD fluxes increasing as ice retreats in the Aurora Subglacial Basin. Our study shows that SFD-enhanced melting is strongly sensitive to meltwater pathways, which are governed by release location and ice-shelf geometry. As a result, evolving drainage configurations, as well as changes in ice-sheet geometry, may substantially modify SFD-driven melting. This highlights the need to incorporate dynamically evolving subglacial hydrology into coupled ice-sheet–ocean models to more realistically capture SFD-driven melting.

The sub-200 m horizontal resolution of our simulations enables us to resolve meltwater layer flow interacting with small-scale ice-draft features, such as basal channels and a detailed grounding line geometry. These features play a key role in controlling the divergence or convergence of meltwater pathways, and thereby how melting scales with SFD. In contrast, such geometric details are poorly represented in studies using coarser-resolution 3D ocean models (Gwyther et al., 2023; Vaňková et al., 2025a) and in current ice-sheet models, which typically operate at resolutions of 2–10 km and lack an explicit representation of meltwater pathways (Seroussi et al., 2024). These limitations suggest that key processes controlling meltwater pathways are likely to be missed in coarser model setups or models that rely on coarser ice geometry data, despite their potentially large influence on total melt rates. This highlights the need for the development of parameterizations that can capture these processes in coarser-resolution frameworks, or, alternatively, the need for higher-resolution models. For the latter, higher resolution may be needed only on the ice-sheet side, with LADDIE potentially serving as an interface between coarser-resolution ocean model data and high-resolution ice-sheet geometry.

Such an approach, however, relies on coarser-resolution ocean forcing that can be reliably extrapolated into the cavity. In our evaluation, we intentionally forced LADDIE with detailed in-cavity conditions from MITgcm, in order to assess the SFD representation under prescribed in-cavity ocean conditions. However, such detailed in-cavity conditions are rarely available in practice. Instead, LADDIE would typically be forced with temperature and salinity fields derived from ice front conditions or coarser-resolution ocean models, which may not accurately represent conditions within the ice-shelf cavity. In these settings, calibrating LADDIE (e.g., its drag coefficient) against observations while including SFD requires care, because uncertainty in the in-cavity conditions can affect melt to a similar extent as the SFD itself.

8. Conclusions

In this study, we modified the meltwater-layer model LADDIE to include subglacial freshwater discharge (SFD). We show that LADDIE quantitatively reproduces key features of SFD-enhanced melting simulated by the more complex 3D ocean model MITgcm, demonstrating its ability to capture the main physical processes at reduced computational cost, thereby offering a promising way to better represent SFD-enhanced sub-shelf melting in ice-sheet models.

Our simulations for Thwaites and Pine Island indicate a strong sensitivity of SFD-enhanced melting, both in spatial pattern and integrated magnitude, to the release location. A more divergent meltwater pathway leads to a larger increase in integrated melting compared to more convergent pathways. This occurs because a distributed buoyancy forcing over a larger area enhances friction velocities and thus melting more effectively than a concentrated input over a smaller area.

21699291, 2026, 12, Downloaded from https://agupubs.onlinelibrary.wiley.com/doi/10.1029/2026JC024641 by British Antarctic Survey, Wiley Online Library on [27/11/2026]. See the Terms and Conditions (https://onlinelibrary.wiley.com/terms-and-conditions) on Wiley Online Library for rules of use; OA articles are governed by the applicable Creative Commons License

21699291, 2026, 12, Downloaded from https://agupubs.onlinelibrary.wiley.com/doi/10.1029/2026JC024641 by British Antarctic Survey, Wiley Online Library on [27/11/2026]. See the Terms and Conditions (https://onlinelibrary.wiley.com/terms-and-conditions) on Wiley Online Library for rules of use; OA articles are governed by the applicable Creative Commons License

Regarding the impact on ice dynamics, variations in the spatial distribution of melt are likely to be more relevant than changes in integrated melt alone. Our results show that different release locations and widths can strongly modify melt patterns, and in some cases focus SFD-driven melt anomalies in regions that contribute disproportionately to ice-shelf buttressing while only modestly affecting integrated melt.

Across the explored ambient ocean states, the additional melting induced by SFD varies only moderately in both pattern and integrated magnitude. Taken together, for substantial SFD forcing and neglecting coupled feedbacks between SFD and ambient ocean conditions, our results indicate that the release location and the downstream meltwater pathway exert a stronger control on SFD-enhanced melting than background ocean conditions.

Accurately representing SFD release locations and downstream meltwater pathways is therefore essential for realistically capturing SFD-enhanced melting. This highlights the need for continued efforts to constrain SFD locations using both observations and subglacial hydrology models, and to adequately resolve meltwater pathways in coupled ice-sheet–ocean models. Progress on both fronts will depend on more accurate, well-constrained ice and bed geometry data.

Appendix A: LADDIE Model Parameters

Table A1.

Table A1
Model Parameters Used in This Study's Configuration of LADDIE

Parameter	Description	Default value	Unit
g	gravitational acceleration	9.81	m s^{-2}
ρ_0	reference seawater density	1,028	kg m^{-3}
$C_{d,\mathrm{mom}}$	momentum drag coefficient	2.5×10^{-3}	–
$C_{d,\mathrm{top}}$*	top drag coefficient	2.5×10^{-3}	–
α	thermal expansion coefficient	3.733×10^{-5}	°C^{-1}
β	haline contraction coefficient	7.843×10^{-4}	psu^{-1}
C_p	heat capacity of seawater	3,974	J kg^{-1} °C^{-1}
L	latent heat of fusion	3.34×10^5	J kg^{-1}
C_I	heat capacity of ice	2,009	J kg^{-1} °C^{-1}
λ_1	PMP salinity parameter	-5.73×10^{-2}	°C psu^{-1}
λ_2	PMP offset parameter	8.32×10^{-2}	°C
λ_3	PMP depth parameter	7.61×10^{-4}	°C m^{-1}
ν_0	kinematic viscosity	1.95×10^{-6}	$m^2 s^{-1}$
Pr	molecular Prandtl number	13.8	–
Sc	molecular Schmidt number	2,432	–
μ	entrainment parameter	2.5	–
H_{min}	minimum layer thickness	1.0	m

Note. PMP = pressure melting point. Parameters marked with * denote deviations from the setup in Lambert et al. (2026).

Conflict of Interest

The authors declare no conflicts of interest relevant to this study.

Availability Statement

The LADDIE model code, along with the supporting data and analysis scripts, is available via Jesse (2026).

Acknowledgments
We are grateful to the two anonymous reviewers for their thorough assessment of the manuscript and their constructive feedback, which helped improve the paper. We also thank the editor, Anna Wåhlin, for handling the manuscript and facilitating the review process. FJ was funded by Utrecht University. EL was funded by the Knowledge Programme Sea Level Rise, which received funding from the Dutch Ministry of Infrastructure and Water Management. PRH was funded by the UK Natural Environment Research Council. KAN was funded by the UK Natural Environment Research Council through the TerraFIRMA project. CJB was supported by NWO under Grant OCENW. KLEIN.515. This work used the Dutch national e-infrastructure with the support of the SURF Cooperative using Grant EINF-14151.

References

Adusumilli, S., Fricker, H. A., Medley, B., Padman, L., & Siegfried, M. R. (2020). Interannual variations in meltwater input to the Southern Ocean from Antarctic ice shelves. *Nature Geoscience*, *13*(9), 616–620. https://doi.org/10.1038/s41561-020-0616-z

Alley, K. E., Scambos, T. A., & Alley, R. B. (2022). The role of channelized basal melt in ice-shelf stability: Recent progress and future priorities. *Annals of Glaciology*, *63*(87–89), 18–22. https://doi.org/10.1017/aog.2023.5

Beckmann, J., Reese, R., McCormack, F. S., Cook, S., Bird, L., Gwyther, D., et al. (2025). Disentangling uncertainty in ISMIP6 Antarctic sub-shelf melting and 2300 sea level rise projections. *EGUsphere*, 1–45. https://doi.org/10.5194/egusphere-2025-4069

Berends, C. J., Azizi, V., Bernales, J. A., & van de Wal, R. S. W. (2025). The Utrecht finite volume ice-sheet model (UFEMISM) version 2.0 – Part 1: Description and idealised experiments. *Geoscientific Model Development*, *18*(12), 3635–3659. https://doi.org/10.5194/gmd-18-3635-2025

Bevan, S. L., Luckman, A. J., Benn, D. I., Adusumilli, S., & Crawford, A. (2021). Brief communication: Thwaites Glacier cavity evolution. *The Cryosphere*, *15*(7), 3317–3328. https://doi.org/10.5194/tc-15-3317-2021

Dow, C. F., McCormack, F. S., Young, D. A., Greenbaum, J. S., Roberts, J. L., & Blankenship, D. D. (2020). Totten Glacier subglacial hydrology determined from geophysics and modeling. *Earth and Planetary Science Letters*, *531*, 115961. https://doi.org/10.1016/j.epsl.2019.115961

Dupont, T. K., & Alley, R. B. (2005). Assessment of the importance of ice-shelf buttressing to ice-sheet flow. *Geophysical Research Letters*, *32*(4). https://doi.org/10.1029/2004GL022024

Dutrieux, P., De Rydt, J., Jenkins, A., Holland, P. R., Ha, H. K., Lee, S. H., et al. (2014). Strong sensitivity of pine Island ice-shelf melting to climatic variability. *Science*, *343*(6167), 174–178. https://doi.org/10.1126/science.1244341

Ehrenfeucht, S., Dow, C., McArthur, K., Morlighem, M., & McCormack, F. S. (2025). Antarctic wide subglacial hydrology modeling. *Geophysical Research Letters*, *52*(1), e2024GL111386. https://doi.org/10.1029/2024GL111386

Gladish, C. V., Holland, D. M., Holland, P. R., & Price, S. F. (2012). Ice-shelf basal channels in a coupled ice/ocean model. *Journal of Glaciology*, *58*(212), 1227–1244. https://doi.org/10.3189/2012JoG12J003

Goldberg, D. N., Twelves, A. G., Holland, P. R., & Wearing, M. G. (2023). The non-local impacts of antarctic subglacial runoff. *Journal of Geophysical Research: Oceans*, *128*(10), e2023JC019823. https://doi.org/10.1029/2023JC019823

Gourmelen, N., Jakob, L., Holland, P. R., Dutrieux, P., Goldberg, D., Bevan, S., et al. (2025). The influence of subglacial lake discharge on Thwaites Glacier ice-shelf melting and grounding-line retreat. *Nature Communications*, *16*(1), 2272. https://doi.org/10.1038/s41467-025-57417-1

Gudmundsson, G. H., Barnes, J. M., Goldberg, D. N., & Morlighem, M. (2023). Limited impact of thwaites ice Shelf on future ice loss from Antarctica. *Geophysical Research Letters*, *50*(11), e2023GL102880. https://doi.org/10.1029/2023GL102880

Gwyther, D. E., Dow, C. F., Jendersie, S., Gourmelen, N., & Galton-Fenzi, B. K. (2023). Subglacial freshwater drainage increases simulated basal melt of the totten ice Shelf. *Geophysical Research Letters*, *50*(12), e2023GL103765. https://doi.org/10.1029/2023GL103765

Hager, A. O., Hoffman, M. J., Price, S. F., & Schroeder, D. M. (2022). Persistent, extensive channelized drainage modeled beneath Thwaites Glacier, West Antarctica. *The Cryosphere*, *16*(9), 3575–3599. https://doi.org/10.5194/tc-16-3575-2022

Hewitt, I. J. (2011). Modelling distributed and channelized subglacial drainage: The spacing of channels. *Journal of Glaciology*, *57*(202), 302–314. https://doi.org/10.3189/002214311796405951

Hewitt, I. J. (2020). Subglacial plumes. *Annual Review of Fluid Mechanics*, *52*(1), 145–169. https://doi.org/10.1146/annurev-fluid-010719-060252

Holland, D. M., & Jenkins, A. (1999). Modeling thermodynamic ice–ocean interactions at the base of an ice Shelf. https://doi.org/10.1175/1520-0485(1999)029⟨1787:MTIOIA⟩2.0.CO;2

Holland, P. (2017). The transient response of ice Shelf melting to ocean change. https://doi.org/10.1175/JPO-D-17-0071.1

Holland, P., Bevan, S. L., & Luckman, A. J. (2023). Strong ocean melting feedback during the recent retreat of thwaites Glacier. *Geophysical Research Letters*, *50*(8), e2023GL103088. https://doi.org/10.1029/2023GL103088

Holland, P., & Feltham, D. L. (2006). The effects of rotation and ice Shelf topography on Frazil-Laden ice Shelf water plumes. *Journal of Physical Oceanography*, *36*(12), 2312–2327. https://doi.org/10.1175/JPO2970.1

Jackson, R. H., Motyka, R. J., Amundson, J. M., Abib, N., Sutherland, D. A., Nash, J. D., & Kienholz, C. (2022). The relationship between submarine melt and subglacial discharge from observations at a tidewater glacier. *Journal of Geophysical Research: Oceans*, *127*(10), e2021JC018204. https://doi.org/10.1029/2021JC018204

Jenkins, A., Nicholls, K. W., & Corr, H. F. J. (2010). Observation and parameterization of ablation at the base of Ronne Ice Shelf, Antarctica. *Journal of Physical Oceanography*, *40*(10), 2298–2312. https://doi.org/10.1175/2010JPO4317.1

Jesse, F. (2026). Data supporting "Meltwater pathways control the effect of subglacial discharge on sub-shelf melting". https://doi.org/10.5281/zenodo.23800433

Jesse, F., Lambert, E., & van de Wal, R. S. W. (2025). Sub-shelf melt pattern and ice sheet mass loss governed by meltwater flow below ice shelves. *The Cryosphere*, *19*(9), 3849–3872. https://doi.org/10.5194/tc-19-3849-2025

Jourdain, N. C., Asay-Davis, X., Hattermann, T., Straneo, F., Seroussi, H., Little, C. M., & Nowicki, S. (2020). A protocol for calculating basal melt rates in the ISMIP6 Antarctic ice sheet projections. *The Cryosphere*, *14*(9), 3111–3134. https://doi.org/10.5194/tc-14-3111-2020

Kimura, S., Holland, P. R., Jenkins, A., & Piggott, M. (2014). The effect of meltwater plumes on the melting of a vertical Glacier face. *Journal of Physical Oceanography*, *44*(12), 3099–3117. https://doi.org/10.1175/JPO-D-13-0219.1

Kimura, S., Jenkins, A., Regan, H., Holland, P. R., Assmann, K. M., Whitt, D. B., et al. (2017). Oceanographic controls on the variability of ice-shelf basal melting and circulation of glacial meltwater in the Amundsen Sea embayment, Antarctica. *Journal of Geophysical Research: Oceans*, *122*(12), 10131–10155. https://doi.org/10.1002/2017JC012926

Lambert, E., & Burgard, C. (2025). Brief communication: Sensitivity of Antarctic ice shelf melting to ocean warming across basal melt models. *The Cryosphere*, *19*(7), 2495–2505. https://doi.org/10.5194/tc-19-2495-2025

Lambert, E., Jesse, F., & Berends, C. J. (2026). The one-Layer Antarctic model for Dynamical downscaling of Ice–ocean exchanges (LADDIE) version 2.0. *Geoscientific Model Development*, *19*(19), 9441–9461. https://doi.org/10.5194/gmd-19-9441-2026

Lambert, E., Jüling, A., van de Wal, R. S. W., & Holland, P. R. (2023). Modelling Antarctic ice shelf basal melt patterns using the one-layer Antarctic model for dynamical downscaling of ice–ocean exchanges (LADDIE v1.0). *The Cryosphere*, *17*(8), 3203–3228. https://doi.org/10.5194/tc-17-3203-2023

Le Brocq, A. M., Ross, N., Griggs, J. A., Bingham, R. G., Corr, H. F. J., Ferraccioli, F., et al. (2013). Evidence from ice shelves for channelized meltwater flow beneath the Antarctic Ice Sheet. *Nature Geoscience*, *6*(11), 945–948. https://doi.org/10.1038/ngeo1977

Lewis, E. L., & Perkin, R. G. (1986). Ice pumps and their rates. *Journal of Geophysical Research*, *91*(C10), 11756–11762. https://doi.org/10.1029/JC091iC10p11756

Lowery, K., Holland, P. R., Dutrieux, P., Hogg, A. E., & Gourmelen, N. (2026). Drivers of basal melt variability for pine Island Glacier Ice Shelf: Ocean forcing versus geometric feedback. *Geophysical Research Letters*, *53*(10), e2025GL121404. https://doi.org/10.1029/2025GL121404

21699291, 2026, 12, Downloaded from https://agupubs.onlinelibrary.wiley.com/doi/10.1029/2026JC024641 by British Antarctic Survey, Wiley Online Library on [27/11/2026]. See the Terms and Conditions (https://onlinelibrary.wiley.com/terms-and-conditions) on Wiley Online Library for rules of use; OA articles are governed by the applicable Creative Commons License

Lowery, K., Sun, S., Dutrieux, P., Holland, P., De Rydt, J., Gourmelen, N., et al. (n.d.). Recent changes in the stress regime and buttressing of Pine Island Glacier. *Geophysical Research Letters*. Manuscript in review.

Malczyk, G., Gourmelen, N., Werder, M., Wearing, M., & Goldberg, D. (2023). Constraints on subglacial melt fluxes from observations of active subglacial lake recharge. *Journal of Glaciology*, *69*(278), 1900–1914. https://doi.org/10.1017/jog.2023.70

Morlighem, M., Goldberg, D., Dias dos Santos, T., Lee, J., & Sagebaum, M. (2021). Mapping the sensitivity of the Amundsen Sea embayment to changes in external forcings using automatic differentiation. *Geophysical Research Letters*, *48*(23), e2021GL095440. https://doi.org/10.1029/2021GL095440

Morlighem, M., Rignot, E., Binder, T., Blankenship, D., Drews, R., Eagles, G., et al. (2020). Deep glacial troughs and stabilizing ridges unveiled beneath the margins of the Antarctic ice sheet. *Nature Geoscience*, *13*(2), 132–137. https://doi.org/10.1038/s41561-019-0510-8

Nakayama, Y., Cai, C., & Seroussi, H. (2021). Impact of subglacial freshwater discharge on Pine Island Ice Shelf. *Geophysical Research Letters*, *48*(18), e2021GL093923. https://doi.org/10.1029/2021GL093923

Naughten, K. A., Holland, P. R., & De Rydt, J. (2023). Unavoidable future increase in West Antarctic ice-shelf melting over the twenty-first century. *Nature Climate Change*, *13*(11), 1222–1228. https://doi.org/10.1038/s41558-023-01818-x

Otosaka, I. N., Shepherd, A., Amory, C., Horwath, M., Ivins, E. R., King, M. D., et al. (2026). Mass balance of the Greenland and Antarctic ice sheets from the 1970s to 2023. *Scientific Data*, *13*(1), 1301. https://doi.org/10.1038/s41597-026-08088-0

Pelle, T., Greenbaum, J. S., Ehrenfeucht, S., Dow, C. F., & McCormack, F. S. (2024). Subglacial discharge accelerates dynamic retreat of Aurora subglacial Basin outlet glaciers, East Antarctica, over the 21st century. *Journal of Geophysical Research: Earth Surface*, *129*(7), e2023JF007513. https://doi.org/10.1029/2023JF007513

Prakash, A., Zhou, Q., Hattermann, T., & Kirchner, N. (2025). Enhanced subglacial discharge amplifies Petermann Ice Shelf melting when ocean thermal forcing saturates. *Nature Communications*, *16*(1), 4213. https://doi.org/10.1038/s41467-025-59469-9

Reese, R., Gudmundsson, G. H., Levermann, A., & Winkelmann, R. (2018). The far reach of ice-shelf thinning in Antarctica. *Nature Climate Change*, *8*(1), 53–57. https://doi.org/10.1038/s41558-017-0020-x

Reese, R., Jourdain, N. C., Asay-Davis, X. S., Burgard, C., Lambert, E., Nakayama, Y., et al. (2026). A protocol for calibrating basal melt rates in the ISMIP7 Antarctic ice sheet projections. *EGUsphere*, *1–56*. https://doi.org/10.5194/egusphere-2026-5337

Rignot, E., Mouginot, J., Scheuchl, B., van den Broeke, M., van Wessem, M. J., & Morlighem, M. (2019). Four decades of Antarctic Ice Sheet mass balance from 1979–2017. *Proceedings of the National Academy of Sciences*, *116*(4), 1095–1103. https://doi.org/10.1073/pnas.1812883116

Seroussi, H., Pelle, T., Lipscomb, W. H., Abe-Ouchi, A., Albrecht, T., Alvarez-Solas, J., et al. (2024). Evolution of the antarctic ice sheet over the next three centuries from an ISMIP6 model ensemble. *Earth's Future*, *12*(9), e2024EF004561. https://doi.org/10.1029/2024EF004561

Shepherd, A., Gilbert, L., Muir, A. S., Konrad, H., McMillan, M., Slater, T., et al. (2019). Trends in antarctic ice sheet elevation and mass. *Geophysical Research Letters*, *46*(14), 8174–8183. https://doi.org/10.1029/2019GL082182

Slater, D. A., Nienow, P. W., Cowton, T. R., Goldberg, D. N., & Sole, A. J. (2015). Effect of near-terminus subglacial hydrology on tidewater glacier submarine melt rates. *Geophysical Research Letters*, *42*(8), 2861–2868. https://doi.org/10.1002/2014GL062494

Vaňková, I., Asay-Davis, X., Branecky Begeman, C., Comeau, D., Hager, A., Hoffman, M., et al. (2025a). Subglacial discharge effects on antarctic ice-shelf basal melt and the Southern Ocean in a global, coupled Ocean—Sea-Ice model. *Journal of Geophysical Research: Oceans*, *130*(10), e2025JC022999. https://doi.org/10.1029/2025JC022999

Vaňková, I., Asay-Davis, X., Branecky Begeman, C., Comeau, D., Hager, A., Hoffman, M., et al. (2025b). Subglacial discharge effects on basal melting of a rotating, idealized ice shelf. *The Cryosphere*, *19*(1), 507–523. https://doi.org/10.5194/tc-19-507-2025

Vreugdenhil, C. A., & Taylor, J. R. (2019). Stratification effects in the turbulent boundary layer beneath a melting ice Shelf: Insights from resolved large-eddy simulations. *Journal of Physical Oceanography*, *49*(7), 1905–1925. https://doi.org/10.1175/JPO-D-18-0252.1

Wåhlin, A. K., Graham, A. G. C., Hogan, K. A., Queste, B. Y., Boehme, L., Larter, R. D., et al. (2021). Pathways and modification of warm water flowing beneath Thwaites Ice Shelf, West Antarctica. *Science Advances*, *7*(15), eabd7254. https://doi.org/10.1126/sciadv.abd7254

Wearing, M. G., Dow, C. F., Goldberg, D. N., Gourmelen, N., Hogg, A. E., & Jakob, L. (2024). Characterizing subglacial hydrology within the amery ice Shelf catchment using numerical modeling and satellite altimetry. *Journal of Geophysical Research: Earth Surface*, *129*(4), e2023JF007421. https://doi.org/10.1029/2023JF007421

Wearing, M. G., Stevens, L. A., Dutrieux, P., & Kingslake, J. (2021). Ice-Shelf basal melt channels stabilized by secondary flow. *Geophysical Research Letters*, *48*(21), e2021GL094872. https://doi.org/10.1029/2021GL094872

Webber, B. G. M., Heywood, K. J., Stevens, D. P., Dutrieux, P., Abrahamsen, E. P., Jenkins, A., et al. (2017). Mechanisms driving variability in the ocean forcing of Pine Island Glacier. *Nature Communications*, *8*(1), 14507. https://doi.org/10.1038/ncomms14507

Wei, W., Blankenship, D. D., Greenbaum, J. S., Gourmelen, N., Dow, C. F., Richter, T. G., et al. (2020). Getz Ice Shelf melt enhanced by freshwater discharge from beneath the West Antarctic Ice Sheet. *The Cryosphere*, *14*(4), 1399–1408. https://doi.org/10.5194/tc-14-1399-2020

Wekerle, C., McPherson, R., von Appen, W.-J., Wang, Q., Timmermann, R., Scholz, P., et al. (2024). Atlantic Water warming increases melt below Northeast Greenland's last floating ice tongue. *Nature Communications*, *15*(1), 1336. https://doi.org/10.1038/s41467-024-45650-z

Wild, C. T., Snow, T., Dotto, T. S., Davis, P. E. D., Tyler, S., Scambos, T. A., et al. (2025). Thwaites Eastern Ice Shelf cavity observations reveal multiyear sea ice dynamics and deepwater warming in Pine Island Bay, West Antarctica. *Ocean Science*, *21*(5), 2605–2629. Retrieved from https://os.copernicus.org/articles/21/2605/2025/doi:10.5194/os-21-2605-2025

Xu, Y., Rignot, E., Menemenlis, D., & Koppes, M. (2012). Numerical experiments on subaqueous melting of Greenland tidewater glaciers in response to ocean warming and enhanced subglacial discharge. *Annals of Glaciology*, *53*(60), 229–234. https://doi.org/10.3189/2012AoG60A139

Zhang, Y., Moore, J. C., Zhao, L., Werder, M. A., Gladstone, R., & Wolovick, M. (2024). The role of hydraulic conductivity in the Pine Island Glacier's subglacial water distribution. *Science of The Total Environment*, *927*, 172144. https://doi.org/10.1016/j.scitotenv.2024.172144

Zinck, A.-S. P., Lhermitte, S., Wearing, M. G., & Wouters, B. (2026). Channelized melt beneath Antarctic ice shelves previously underestimated. *Nature Climate Change*, *16*(3), 1–4. https://doi.org/10.1038/s41558-025-02537-1

21699291, 2026, 12, Downloaded from https://agupubs.onlinelibrary.wiley.com/doi/10.1029/2026JC024641 by British Antarctic Survey, Wiley Online Library on [27/11/2026]. See the Terms and Conditions (https://onlinelibrary.wiley.com/terms-and-conditions) on Wiley Online Library for rules of use; OA articles are governed by the applicable Creative Commons License